

CDM-variant cosmological models – I: Simulations and preliminary comparisons

Michael A. K. Gross,^{1,2*} Rachel S. Somerville,^{1,3*} Joel R. Primack,^{1*}
Jon Holtzman^{4*} and Anatoly Klypin^{4*}

¹Physics Department, University of California, Santa Cruz, CA 95064 USA

²NASA/Goddard Space Flight Center, Code 931, Greenbelt, MD 20771 USA

³Racah Institute of Physics, The Hebrew University, Jerusalem 91904, Israel

⁴Department of Astronomy, New Mexico State University, Las Cruces, NM 88001 USA

2 December 2024

ABSTRACT

We present two matched sets of five simulations each, covering five presently favored simple modifications to the standard cold dark matter (CDM) scenario. One simulation suite, with a linear box size of $75 h^{-1}$ Mpc, is designed for high resolution and good statistics on the group/poor cluster scale, and the other, with a box size of $300 h^{-1}$ Mpc, is designed for good rich cluster statistics. All runs had 57 million cold particles, and models with massive neutrinos had an additional 113 million hot particles. We consider separately models with massive neutrinos, tilt, curvature, and a nonzero cosmological constant ($\Lambda \equiv 3H_0^2\Omega_\Lambda$) in addition to the standard CDM model. We find that our tilted $\Omega_0 + \Omega_\Lambda = 1$ (Λ CDM) model produces too much small-scale power by a factor of ~ 3 , and our open $\Lambda = 0$ (OCDM) model also exceeds observed small-scale power by a factor of 2. In addition, we take advantage of the large dynamic range in detectable halo masses our simulations allow to check the shape of the Press-Schechter approximation. We find good fits at cluster masses for $\delta_{c,g} = 1.27\text{--}1.35$ for a Gaussian filter and $\delta_{c,t} = 1.57\text{--}1.73$ for a tophat filter. However, Press-Schechter overpredicts the number density of halos compared to the simulations in the high resolution suite by a weakly cosmology-dependent factor of 1.5–2 at galaxy and group masses, which cannot be fixed by adjusting δ_c within reasonable bounds. An appendix generalizes the spherical collapse model to any isotropic cosmology.

Key words: large-scale structure of universe – dark matter – cosmology:theory – cosmic microwave background

1 INTRODUCTION

The *COBE* DMR detection of anisotropies in the cosmic microwave background (Smoot et al. 1992) made it very clear that the ‘standard’ structure formation scenario of cold dark matter (Blumenthal et al. 1984; Davis et al. 1985) cannot simultaneously account for fluctuations on very large and very small scales. That model made several very restrictive assumptions about cosmological parameters – that space-time is homogenous, isotropic and globally flat; that there is no cosmological constant; that fluctuations from homogeneity are Gaussian-distributed and nearly scale-independent at horizon crossing; that the Hubble parameter $h \equiv H_0 /$

($100 \text{ km s}^{-1} \text{ Mpc}^{-1}$) is 0.5; and that the number of free parameters is minimized. The obvious fixes to the problem of excess small-scale power (when normalizing power spectra to the *COBE* anisotropy) are to make one of the following modifications to the model:

- (i) tilt the primordial spectrum,
- (ii) allow a nonzero cosmological constant but retain globally flat geometry,
- (iii) allow the universe to be open,
- (iv) add hot dark matter (i.e., neutrinos with masses of a few eV), or
- (v) lower the Hubble parameter much further ($h \sim 0.3\text{--}0.4$).

Each of these modifications adds only one free parameter to the cosmology. In this paper, we consider the most viable models from each class above except the last, and simulate

* E-mail: gross@fizzie.gsfc.nasa.gov (MAKG);
rachels@alf.fiz.huji.ac.il (RSS); joel@ucolick.org (JRP);
holtz@nmsu.edu (JH); aklypin@nmsu.edu (AK)

them with an N -body code in two suites, with equivalent initial conditions across all the models. We do not consider a ‘low- H_0 ’ model (Bartlett et al. 1995) because of increasingly solid observational evidence that $h \gtrsim 0.5$.

Deciding on cosmological parameters is to some extent an iterative process. Much can be done using the Press-Schechter (1974) approximation, but the assumptions that go into it are not necessarily realistic (for example, spherical symmetry – see Jain & Bertschinger 1994 and Monaco 1995). Therefore, it is useful as a *first approximation* to calculating the mass functions, and we use it to perform an approximate cluster normalization, using guesses about other cosmological parameters. We run a set of simulations and use them to verify the Press-Schechter approximation, and make several preliminary comparisons to observational data. In a companion paper (Gross et al. 1997), we recalibrate the Press-Schechter approximation and use it to derive refined estimates of model normalization and Ω_0 from several different data sets, and make more careful comparisons to cluster abundance. Subsequent papers will use simulations based on the refined normalizations.

In section 2.1, we describe the specific models from each class of CDM-variant models and explain why we chose the parameters as we did. In section 2.2, we briefly describe the modifications to the particle-mesh algorithm we made for this study. We explain our halo finding algorithm and the effect of mass resolution upon it in section 3 and report the simulation results in section 4. Finally, in section 5, we give our conclusions.

2 SIMULATIONS

2.1 Models

Given the long list of modifications to the cold dark matter scenario in the previous section, we could construct a model that tweaked *every* parameter, to try to make a best-fit universe to all the observational data available. But, such an ‘epicycle’ model would be ugly. So, we try to minimize the number of modifications to the relatively simple standard cold dark matter scenario, considered at one time, except that we allow a small tilt to $n = 0.9$ in each model in addition to modifications (ii)–(iv), in order to be consistent with both *COBE* and cluster abundances. Larger tilts are not allowed because they tend to cause disagreements with high-multipole cosmic microwave background data.

We constrain models by running a large suite of linear calculations and comparing the output to appropriate observational constraints. Constraints that we consider in choosing model parameters for more detailed nonlinear analysis are:

(i) the abundance of Abell clusters, as measured by X-ray temperature profiles (White, Efstathiou, & Frenk 1993; Biviano et al. 1993, hereafter WEF93 and BGGMM93, respectively). We allow for cluster masses to be underestimated by up to a factor of two due to results from cluster density mapping with gravitational lensing (Squires et al. 1996; Squires et al. 1997; Miralda-Escudé & Babul 1995; Wu & Fang 1996; Wu & Fang 1997; figure 1),

(ii) microwave background anisotropies for $\ell \lesssim 800$ (figure 2) as measured by several recent CMB detection exper-

iments (Tegmark 1996; Netterfield et al. 1997; Scott et al. 1996; Platt et al. 1997; figure 2)

(iii) ‘bulk flow’ peculiar velocity measurements and resulting constraints on the power spectrum (Dekel et al. 1997; Kolatt & Dekel 1997; figure 4). The linear estimates of these parameters are shown in table 1 and in figures 1, 2, and 4 for the models we consider.

For most models, we presume a baryon abundance of $\Omega_b = 0.025h^{-2}$, consistent with the Tytler, Fan, & Burles (1996) cosmic deuterium abundance measurement. Normalization is accomplished by calculating low multipoles using an enhanced version of the linear code from Holtzman (1989) and comparing to the four-year *COBE* DMR anisotropy measurements (Górski et al. 1996; Górski, private communication).

For comparison to other studies, we also simulated the standard cold dark matter (SCDM) model with bias $b = \sigma_8^{-1} = 1.5$.¹ That model is intended to approximately match observed cluster abundances on small scales at the cost of being inconsistent with the *COBE* anisotropy measurements. For this model, we presumed there were no baryons in the Universe, and used the BBKS transfer function (Bardeen et al. 1986) used in previous studies, that is,

$$P(k) = Ak \frac{[\ln(1 + 2.34q)]^2}{(2.34q)^2} \times (1 + 3.89q + (16.1q)^2 + (5.46q)^3 + (6.71q)^4)^{-1/2} \quad (1)$$

with $q = kh^{-2}$ and A adjusted so that the rms fractional variance in mass in spheres of radius $8 h^{-1}$ Mpc estimated using linear theory is $\sigma_8 = 0.667$.

The simplest method to fix the standard model’s problems at small scales is by ‘tilting’ the spectrum, that is, by changing the Ak factor in equation (1) to Ak^n , with $n < 1$. We find, using Press-Schechter estimates of the cluster abundance (table 1), that with $h = 0.45$, a tilt of $n = 0.9$ with *COBE* normalization

matches the cluster abundance reasonably at $M = 6 \times 10^{14} h^{-1} M_\odot$, so we use these parameters for the tilted case (TCDM).

Another fix is to add a little hot dark matter. The traditional approach for this class of models is to postulate that there is one species of neutrino with significant mass. We find a good match to observed cluster abundances with tilt $n = 0.9$, $h = 0.55$, and $\Omega_\nu = 0.2$. However, if we allow $N_\nu = 2$ species of equal-mass neutrinos, the power on cluster scales is reduced by 20 per cent without affecting smaller or larger scales, which lowers cluster abundances without worsening potential early structure formation problems (small-scale power) or *COBE* normalization (Primack et al. 1995; Pogosyan & Starobinsky 1995). A reasonable model can be constructed either without any tilt ($n = 1$) or with higher h . We choose the former, based on concerns about the age of the Universe.²

¹ In this entire paper, we quote σ_8 as it is estimated from the *linear* approximation, even though the $8 h^{-1}$ Mpc scale is clearly in the nonlinear regime at $z = 0$. Approximate corrections to the nonlinear measurements can be made using the Press-Schechter approximation, but since we never compare σ_8 directly to observations, there is no point in that.

² We ran the simulations before the Hipparcos recalibration of the

Table 1. Model parameters and linear results for both simulation suites.

Model	Age ^a	h^b	Ω_0	Ω_c	Ω_b	Ω_ν	Ω_Λ	n^c	N_ν^d	σ_8^e	$\tilde{\sigma}_8^f$	V_{50}^g	N_{cl}^h
observations												375	5×10^{-6}
1- σ errors												85	2×10^{-6}
CHDM-2 ν	13.0	0.5	1.0	0.7	0.1	0.2	0.	1.	2	0.719	0.719	399	6×10^{-6}
OCDM	12.3	0.6	0.5	0.431	0.069	0.	0.	1.	0	0.773	0.578	254	3×10^{-6}
SCDM	13.0	0.5	1.	1.	0.	0.	0.	1.	0	0.667	0.667	192	2×10^{-6}
TCDM	14.5	0.45	1.	0.9	0.1	0.	0.	0.9	0	0.732	0.732	270	5×10^{-6}
TACDM	14.5	0.6	0.4	0.365	0.035	0.	0.6	0.9	0	0.878	0.572	335	2×10^{-6}

^a Time since the Big Bang in Gyr.

^b Presumed Hubble parameter, in units of $100 \text{ km s}^{-1} \text{ Mpc}^{-1}$.

^c ‘Tilt’ of the primordial spectrum; $P(k) \propto k^n$.

^d Number of massive neutrinos presumed. The equivalent mass of a neutrino is $m_\nu = \frac{\Omega_\nu h^2}{N_\nu} \cdot 92 \text{ eV}$.

^e rms mass fluctuation in a sphere of radius $8 h^{-1} \text{ Mpc}$.

^f $\tilde{\sigma}_8 \equiv \sigma_8 \Omega_0^{0.46-0.10\Omega_0}$ for $\Lambda = 0$ models, and $\sigma_8 \Omega_0^{0.52-0.13\Omega_0}$ for $\Omega_\Lambda + \Omega_0 = 1$ models. Eke, Cole, & Frenk (1996) calculate $\tilde{\sigma}_8 = 0.52 \pm 0.04$ in order to fit cluster temperatures assuming $\beta \equiv \langle KE \rangle_{\text{dm}} / \langle KE \rangle_{\text{gas}} = 1$.

^g rms velocity in a sphere of radius $50 h^{-1} \text{ Mpc}$ (Dekel et al. 1997).

^h Estimated number density of clusters of mass $6 \times 10^{14} h^{-1} M_\odot$, in $h^3 \text{ Mpc}^{-3}$, from Press-Schechter theory with a Gaussian window function. $\delta_{c,g}$ is 1.5 for CHDM models (Walter & Klypin 1996; Borgani et al. 1997b) and 1.3 for all other models (Liddle et al. 1996, KPH96). Masses near the center of the allowable range for cluster data (WEF93, BGGMM93) are used. Note that uncertainties in the masses of measured clusters mean that the masses for which densities were measured could shift coherently up to a factor of two above the reported value of $4.2 \times 10^{14} h^{-1} M_\odot$. This is a naive approach which we use only for our first iteration of model parameters. We use more sophisticated methods in Gross et al. (1997).

We also consider a flat model with a cosmological constant (TACDM), which requires a modest tilt ($n = 0.9$) to get the cluster abundance approximately correct. This particular model is our best candidate model in this class, and we have studied it and many other Λ CDM models previously with smaller simulations (Klypin, Primack, & Holtzman 1996, hereafter KPH96; Smith et al. 1997). As we consider even small simulations to be a more reliable indicator of model efficacy than linear estimates, we choose our candidate model from the simulation pool rather than the linear tables. As a better match to the observed baryon fraction (Ω_b/Ω_0 if the baryon fraction is universal) in clusters in low- Ω_0 models, we use a smaller Ω_b for TACDM than we do in the larger- Ω_0 models.

Many observers favor an open cosmology and a high Hubble parameter, consistent with local density estimates and the Hubble Key Project. The lowest reasonable value of Ω_0 , given initial Gaussian fluctuations as assumed in all CDM-variant models considered here, is constrained to be above 0.3 at $\gtrsim 4\sigma$ confidence (Nusser & Dekel 1993; cf. also Dekel & Rees 1994; Bernardeau et al. 1995). We adopt $\Omega_0 = 0.5$ as a ‘reasonable’ value for OCDM, noting that even this relatively high Ω_0 leads to a power spectrum lower than that indicated by the POTENT analysis (Kolatt & Dekel 1997; see also figure 4). Our choice of Ω_0 for this model and for TACDM is somewhat higher than that used by the Virgo collaboration (Jenkins et al. 1996) for this reason. Our linear code is not capable of determining low multipole cosmic microwave background fluctuations for OCDM, as it uses a plane wave expansion that is only appropriate for flat cos-

mologies. Instead, we use fitting functions for the normalization $\delta_H(\Omega_0)$ and the transfer function $T(k)$ given by Liddle et al. (1996, hereafter LLRV96).³

Figure 1 summarizes the expected mass functions on the group and cluster mass scales, as estimated from the Press-Schechter approximation, with a Gaussian filter. Consistent with results from Borgani et al. (1997b), we use $\delta_{c,g} = 1.5$ for models with massive neutrinos and $\delta_{c,g} = 1.3$ for all other models, in this figure. The observational cluster abundance estimates plotted are in reasonable agreement with these mass functions, especially if the mass estimates are low as indicated by some gravitational lensing estimates.

In figure 2, we compare each model to several recent CMB measurements, using the CMBFAST program of Seljak & Zaldarriaga (1996). We also show the four most recently announced CMB results on the figure. Not shown are systematic calibration errors, so all the Saskatoon points could move up or down coherently by up to 14 per cent, and both the Python III points could move by up to 20 per cent in either direction.

³ After we ran this model, LLRV96 was superseded by Bunn & White (1997) and Hu & White (1997). Those papers’ σ_8 values agree to high precision with LLRV96 if one lowers Ω_b from 0.025 h^{-2} to 0.015 h^{-2} , which Bunn & White (1997) favor anyway. However, the transfer function shapes are somewhat different, and the LLRV96 normalization is to the *COBE* 2-year data, so the power on scales of a few hundred $h^{-1} \text{ kpc}$ may be up to 20 per cent low compared to Bunn & White (1997) and Hu & White (1997). Using a BBKS-style fit as all three papers do, rather than integrating the Boltzmann equation directly, introduces an error of similar magnitude, even with the improved shape parameter described in Hu & Sugiyama (1996, equation D-29). We therefore neglect the difference between the Bunn & White (1997) and LLRV96 spectra.

age of globular clusters (Reid 1997; Gratton et al. 1997; Chaboyer et al. 1997). This constraint has disappeared, and $h = 0.6$ or even 0.65 is perfectly reasonable today.

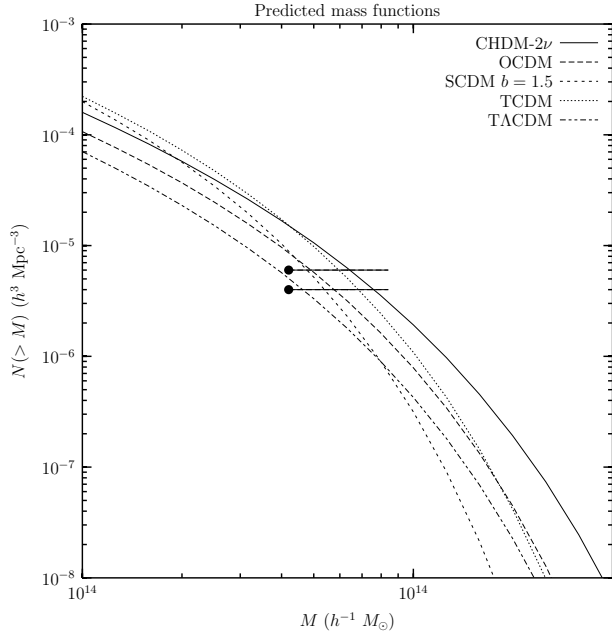


Figure 1. Expected mass functions for all models estimated from the Press-Schechter approximation with a Gaussian filter, using $\delta_{c,g} = 1.5$ for models with massive neutrinos and $\delta_{c,g} = 1.3$ for all other models. The two data points shown correspond to observational estimates of cluster abundance (WEF93, BG-GMM93). Note that cluster density mapping via gravitational lensing (Squires et al. 1996; Squires et al. 1997; Miralda-Escudé & Babul 1995; Wu & Fang 1997) may indicate that X-ray masses are systematically low, and the masses can plausibly be raised by a factor of two, which corresponds to the horizontal line on the right of each cluster data point.

Figure 3 shows all of the power spectra we used, projected forward to the present epoch using linear theory. As one might expect, all the spectra nearly cross at a wavenumber of a few tenths $h \text{ Mpc}^{-1}$, corresponding to cluster scales. Also, we show some of the window functions used in the normalization procedure described above.

In figure 4, we compare our models to the matter power spectrum recently measured from bulk flows by Kolatt & Dekel (1997). We only use the three data points that Kolatt & Dekel use for their own statistical analysis, because for larger wavenumbers smoothing lowers the power significantly. SCDM disagrees at about the 2.5σ level, also reflected in its low value of V_{50} in table 1. OCDM and TACDM disagree because the value of $P(\sim 0.1 h \text{ Mpc}^{-1})$ is fixed by comparing the observed density of clusters (WEF93, BG-GMM93, Borgani et al. 1997a) to the Press-Schechter prediction, and they have low values of $f(\Omega_0, \Lambda) \equiv \dot{D}a/D\dot{a} \approx \Omega_0^{0.6}$, where $D(\Omega_0, \Lambda, t)$ is the linear growth factor and $a(t)$ is the expansion parameter. The combination of cluster abundances and bulk-flow power spectrum measurements favors $f \sim 1$, for the currently favored classes of CDM-variant models.

There is currently significant controversy over the proper normalization of models, and our OCDM and TACDM normalizations are higher than the recent fits reported in Eke, Cole, & Frenk (1996), based on cluster X-ray

temperature distributions (Henry & Arnaud 1991),⁴ though they are consistent with the older analyses of WEF93 and the newer cluster velocity dispersion measurements of Borgani et al. (1997a). Pen (1996) has pointed out that power-law approximations used in Eke, Cole, & Frenk (1996) and WEF93 are good approximations only for $\Omega_0 \approx 1$, and has calculated the correction for an $\Omega_0 = 0.35$ Λ CDM model to be 17 per cent above the Eke, Cole, & Frenk (1996) fit. The conclusions of Pen (1996) have been substantiated by at least two relevant Λ CDM N -body simulations: his own $\Omega_0 = 0.35$ simulation and an $\Omega_0 = 0.3$ simulation from Borgani et al. (1997a). Pen (1996) yields cluster normalizations for our TACDM and OCDM models of $\sigma_8 = 0.92$ and 0.74 , respectively. These normalizations are consistent with those we have chosen (table 1).

2.2 Algorithm

A classic problem with gravitational simulations is the ‘overmerging’ problem, where small scale structure in highly overdense regions is not resolved. Part of the problem is physical – real galaxies form much denser cores than dissipationless halos can, because the baryons can dissipate energy (but cf. Klypin, Gottlöber, & Kravtsov 1997). Aside from that, numerical limitations can make the problem vastly worse. There are two numerical effects to consider: force resolution and sampling of initial conditions and bound structures. Improving either of these requires vast amounts of memory and processing time, so there is an inherent tradeoff.

Recently, the more popular approach has been to improve the forces by using hybrid (Hockney & Eastwood 1988; Couchman 1991; Xu 1995, for example) or adaptive-mesh (Kravtsov, Klypin, & Khokhlov 1997, for example) force solvers, at the expense of either poor sampling of initial fluctuations or small box sizes. We choose a complementary approach, where we try to balance the sampling of density in a large box with the force resolution. We still require a large dynamic range in order to sample small scales well and simultaneously simulate a large volume for comparison to redshift surveys. Since the two requirements imply an enormous number of particles, computer time limitations force us to use the *fastest* code available. We choose a standard particle-mesh (Hockney & Eastwood 1988) algorithm, parallelized to run on a distributed-memory message-passing system.⁵ This type of code produces adequate forces at about 1.5 grid cells (KNP97, Appendix A), but we double this distance to be conservative. So, we require that we have 3^3 times as many grid cells as particles. We choose a grid cell size of $65 h^{-1} \text{ kpc}$, with $N_g = 1152^3$ grid cells and $N_p = 384^3 = 57$ million ‘cold’ particles. For models with massive neutrinos we also add twice as many ‘hot’ particles. Initial conditions were calculated using a parallelized Zel’dovich (1970) approximation. For CHDM models, we started with a uniform grid of

⁴ Note that Henry & Arnaud (1991) had two compensating errors in their analysis: an arithmetical error of a factor of 4.2 and a binning error of a factor of about 4 in the other direction. The errors have been noted in WEF93, Eke, Cole, & Frenk (1996), Viana & Liddle (1996), and Pen (1996).

⁵ Specifically, the Cornell Theory Center SP2, but the code is portable to any system supporting MPI, including heterogeneous workstation clusters and most modern supercomputers.

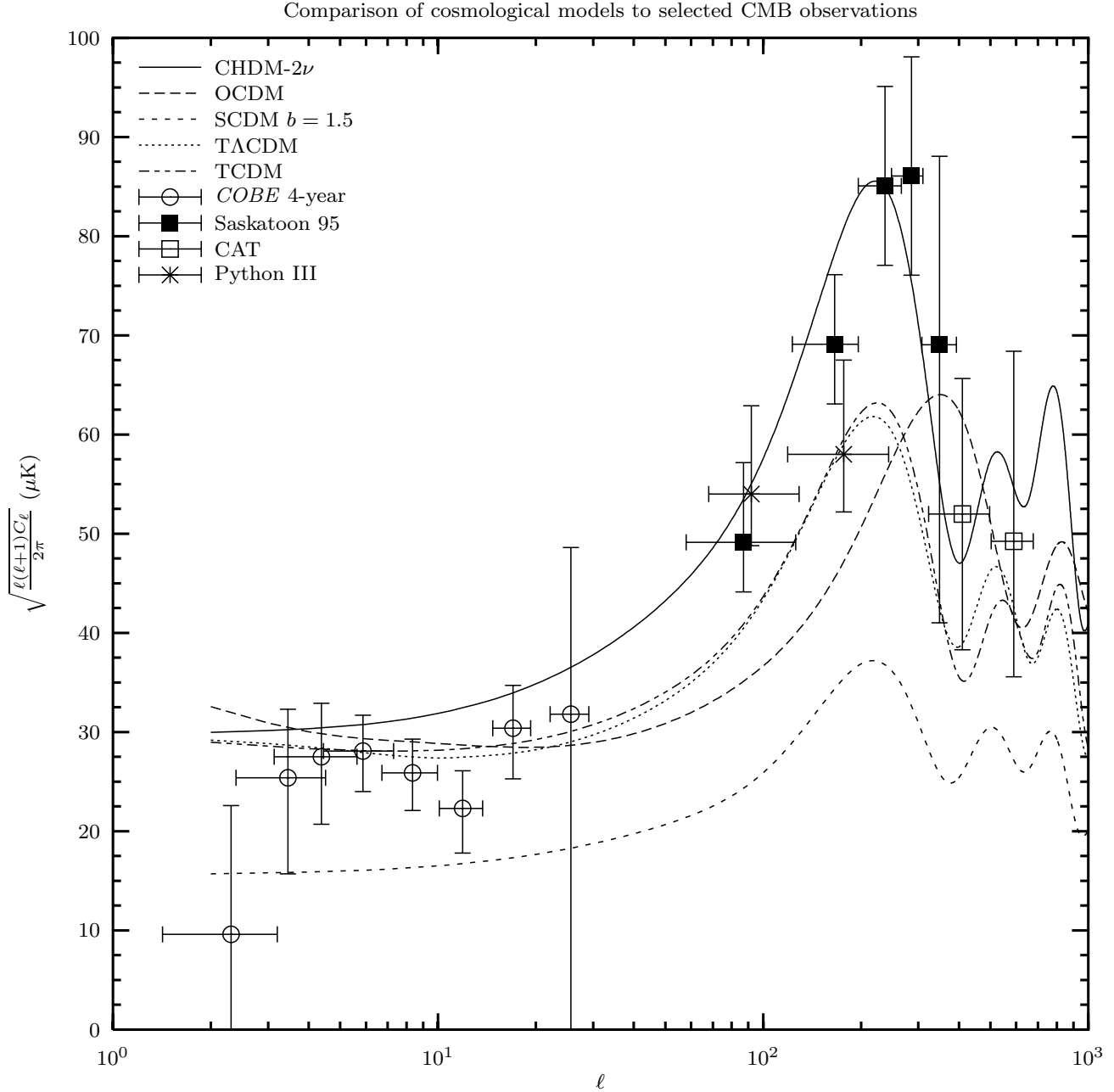


Figure 2. Model Comparison to Cosmic Microwave Background. All models except SCDM are consistent with *COBE* four year data (Górski et al. 1996; Górski, private communication). Circles, solid squares, open squares and asterisks are the *COBE* four year power spectrum (Tegmark 1996), Saskatoon 1995 results (Netterfield et al. 1997), CAT detection (Scott et al. 1996) and Python III results (Platt et al. 1997), respectively. Not shown are systematic normalization errors of 14 and 20 per cent, for Saskatoon and Python III, respectively. The curves are all calculated using the CMBFAST program of Seljak & Zaldarriaga (1996). Cosmological parameters correspond to models considered in this paper, except for SCDM. The normalization is adjusted so that the low harmonics match the output of our linear code. CMBFAST is capable of calculating larger multipoles than our linear code is. SCDM is shown here with $\Omega_b = 0.1$, since all the high- ℓ features in the CMB spectrum are dependent upon baryon interactions, but was actually simulated with no baryons. Note that the OCDM model is strongly inconsistent with the Saskatoon points, and our choice of $\Omega_0 = 0.5$ is the 95 per cent confidence lower limit for an open model (Lineweaver & Barbosa 1997).

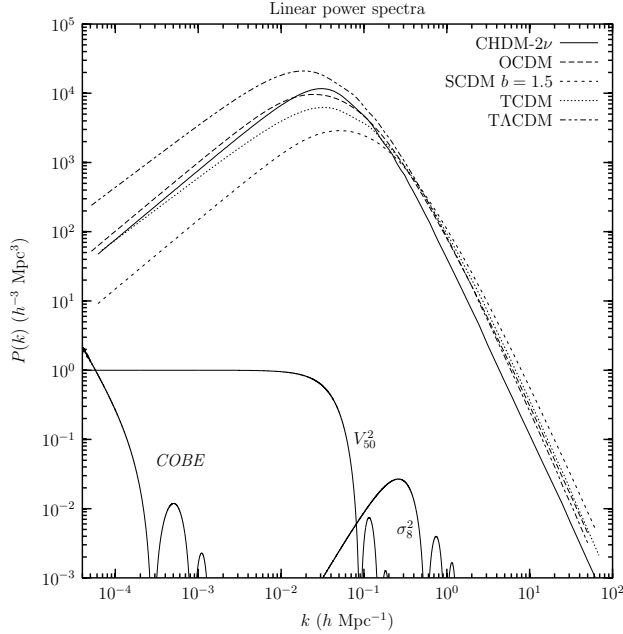


Figure 3. Linear power spectra used in our simulation suites. Also shown are two of the window functions used in normalizing the models: $k^2 W^2(rk)$ with $r = 8 h^{-1} \text{ Mpc}$ for σ_8^2 and $W^2(rk)$ with $r = 50 h^{-1} \text{ Mpc}$ for V_{50}^2 . Here $W(x) = 3[\sin(x) - x \cos(x)]x^{-3}$. Also shown (for illustrative purposes only) is the equivalent window function for approximate *COBE* normalization using the pure Sachs-Wolfe effect, $j_{10}^2(d_h k)/(2\pi d_h^2 k^2)$ where $j_{10}(x)$ is the 10th order spherical Bessel function and d_h is the horizon distance. The version plotted has the amplitude raised by a factor of 100 for visibility and uses $d_h = 2c/H_0 = 6000 h^{-1} \text{ Mpc}$, which is appropriate for $\Omega_0 = 1$. For OCDM, the horizon distance is $7490 h^{-1} \text{ Mpc}$ and for TACDM, it is $8830 h^{-1} \text{ Mpc}$, so the window function moves a small distance to smaller k in those cases. A similar window function for cluster abundance doesn't exist because it doesn't have the form of a convolution. In an extremely rough sense, the scales are comparable to those sampled by σ_8 .

cold particles, and two neutrinos at the position of every cold particle. Cold particles and neutrinos were offset from the grid using separate cold+baryon and hot power spectra, and consistent velocities were derived from the offsets using scale-dependent linear growth rates calculated by a refinement of the Holtzman (1989) code. In addition, equal and opposite random thermal velocities were chosen for each pair of neutrinos from a redshifted relativistic Fermi-Dirac distribution (Klypin et al. 1993).

Such massive simulations could not be run on any single-processor or even shared-memory computer available at the time these simulations were run, as in single precision the particles take 1.3 Gb (4.0 Gb for models with massive neutrinos) and the density grid takes 6.1 Gb of memory for the high resolution suite. That doesn't take into account auxiliary storage needed for finding halos, for example. Also, long running times require large-scale parallelism, as a full-scale run with neutrinos from our high-resolution suite would take about three months on a single-processor IBM RS-6000 model 390, if enough memory could be put into it (it can't). Shared memory machines are better, but not by

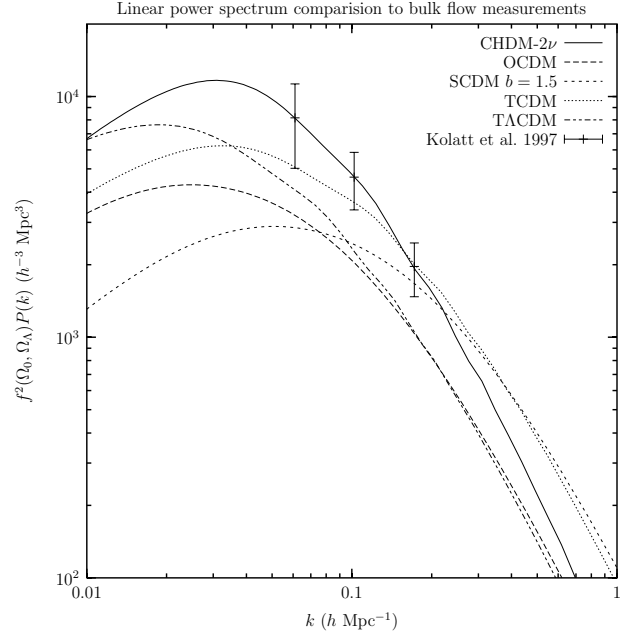


Figure 4. Linear power spectrum comparison to bulk-flow measurements. The curves are all a magnification of figure 3, multiplied by $f^2(\Omega_0, \Omega_\Lambda) \equiv a\dot{D}/\dot{a}D$. The three data points are from Kolatt & Dekel (1997). $f(\Omega_0, \Omega_\Lambda)$ was calculated exactly, using equation (A34) and its analytic derivative.

enough, as coherency and contention problems limited their size to a few dozen processors until very recently,⁶ and they don't quite have enough shared memory. So, we run in about 18 hours on 128 nodes of a distributed memory SP2, with a total available memory of 16 Gb.

The parallelization of a particle-mesh code is much less trivial than one would suppose. Communication is required in every step, and communication optimization must always be done by hand for very large numbers of processors or the speedup will be far less than linear for nontrivial parallelizations.⁷ Since memory is distributed among a very large number of processors, and each processor is far too

⁶ There is at present only one shared-memory supercomputer that is large enough to run the simulations described here. The SGI Origin 2000 is really a distributed-memory computer, but that fact is hidden inside the operating system and one can write *correct* code that ignores that fact. It still has problems with coherency (when two processors write to the same memory at the same time) and contention (when two processors use the same shared resources at the same time). The methods for optimizing for that are very similar to coding for a distributed-memory computer.

⁷ Automatic parallelizers such as Forge can often be beaten by a very large factor of 10 or more since they must necessarily make conservative assumptions about data dependencies and function calls to make correct code. This often results in serializing loops unnecessarily, which can be quite expensive. The very first attempt made with the serial version of our code under Forge was completely unacceptable for this reason. HPF can in principle do much better, but that would require extensive specification of data and loop characteristics, which is as much work as message-passing parallelization.

small to hold the entire density grid or all the particles, one must formulate a scheme for distributing density and particles among the processors. The simplest approach is to give each processor some region of space to compute on and pass particles that leave a given processor’s region to ‘neighboring’ processors. The approach is susceptible to crashing because one processor can use up all its memory, especially at late times when clustering is highly significant. In practice, this severely limits the size of the case that one can run on a given size computer, and no computer in the world is presently large enough to run our suite without crashing given this parallelization, if every processor were responsible for a fixed interval in the z -coordinate, and all values of x and y .

A far less crash-prone scheme is to distribute density according to space, as before, but distribute particles according to *rank* in the z -coordinate, instead of the value. This has the advantage that all processors have exactly the same number of particles, so the sizes of the particle buffers are strictly limited. However, the correspondence between density and particles becomes more complicated because the two quantities may live on different processors in the same region of space. The rank distribution requires sorting the particles, but, with a quicksort followed by interchanging particles in regions where multiple processors have particles, the total time spent in this phase in each timestep is only several per cent of a timestep. The implied search over processors in density and force interpolation is limited in scope because each processor can estimate which others it needs to query before any communication takes place. This is the scheme we use in the simulation suites we report here. Further details are given in Gross (1997).

We adopted the form of the equations of motion used in Kates, Kotok, & Klypin (1991) generalized to arbitrary cosmology:

$$\nabla^2 \phi = \frac{3}{2a} \delta \equiv \frac{3}{2a} \frac{\delta \rho}{\Omega \rho_c}, \quad (2)$$

$$\frac{d\vec{p}_i}{da} = -\dot{a} \vec{\nabla} \phi(\vec{x}_i), \quad (3)$$

and

$$\frac{d\vec{x}_i}{da} = \frac{\vec{p}_i}{a^2 \dot{a}}, \quad (4)$$

where \dot{a} is given by the Friedmann equation with time variable $H_0 t$,

$$\dot{a} = a^{-1/2} \sqrt{\Omega_c + \Omega_\nu + \Omega_\Lambda a^3 + \Omega_k a}. \quad (5)$$

Time discretization was a standard ‘leapfrog’ scheme (cf. Hockney & Eastwood 1988), with even steps in the expansion parameter a . To reduce the expense of the simulations, the timestep was chosen only to stabilize bound structures at the final timestep, rather than keep *all* structures on the scale of the grid spacing stable. This is only a problem for the cores of clusters, which have the highest velocities. For clusters, we presume an upper bound of particle velocities of 1200 km s^{-1} today and a minimum diameter of any given bound structure equal to the linear cell size. Stability for such an object requires that particles take at least one timestep to traverse the object. So, the required condition

is

$$\Delta a \equiv \dot{a} \Delta t \lesssim \frac{H_0 L}{N_g^{1/3} v_{\max}} \quad (6)$$

independent of cosmology because the condition is evaluated at the present epoch and $H_0 L$ is chosen to be the same for all models. Plugging in $v_{\max} = 1200 \text{ km s}^{-1}$, $H_0 L = 7500 \text{ km s}^{-1}$ and $N_g = 1152^3$ gives $\Delta a \lesssim 0.005$, or 200 timesteps for the high resolution suite. Such a low v_{\max} will not model the interiors of clusters well, since they are observed to have velocity dispersions larger than that, but to remain bound to the cluster, particles have the much looser requirement that they not traverse the *whole cluster* in one timestep. As large cluster radii are up to about 50 grid cells, the effective stability limit is 20 per cent the speed of light inside a large cluster, for the high resolution suite, presuming that the cluster is adequately modeled by an isothermal sphere. We checked that the choice of timestep was adequate by running a $25 h^{-1} \text{ Mpc}$ box CHDM- 2ν simulation with 384^3 grid cells (which has the same $65 h^{-1} \text{ kpc}$ cell size as the high resolution suite) for 200 timesteps and for 300 timesteps. The resulting mass functions were not significantly different. For the large volume suite, clusters do not cover nearly as many cells as in the high resolution suite, and so the velocity limit is much higher. Our choice of 150 timesteps corresponds to a limiting speed of 5000 km s^{-1} if particles are not to cross one cell in a timestep. The suite parameters are summarized in table 2

The Zel’dovich (1970) approximation is only valid when the rms fluctuations are much less than 1. In practice, one picks a starting time early enough so that linear theory brings the rms fluctuations well below 1. The initial time was chosen so that the rms overdensity on the grid scale was $\delta_{\text{rms}} \lesssim 0.2$. This was $z = 30\text{--}60$, depending on the model. Particle data and halo catalogs were stored at four equally spaced intervals in a during execution. The large volume simulation suite used the same starting times as the high resolution suite even though they could have been started somewhat later due to the poorer resolution. The extra computation involved is about one timestep and is therefore negligible.

Random numbers are necessary to model inflation-generated Gaussian fluctuations and random phases in the density field. Such randomness introduces highly significant variation from simulation to simulation, commonly referred to as ‘cosmic variance.’ Because we can only observe one universe, quantifying the effect of cosmic variance is very important and is a separate issue from variations between models due to different physics. In these suites, we have separated the effects by picking a single random number seed for each suite, checking that the largest 26 waves do not have any fluctuations larger than a factor of 2, and rerunning one model with a different seed. That is, within each suite, the random numbers for each model within a suite are all the same, and large wavelength fluctuations are restricted to a smaller range than Gaussian statistics would permit, in an attempt to prevent rare statistical flukes from compromising expensive simulations (as happened in Klypin et al. 1993). This means the structures are approximately in the same place, and when one also considers the cluster abundance criterion discussed in section 2.1 there is roughly the same number, distribution and positions of $5 \times 10^{14} h^{-1} M_\odot$ clus-

Table 2. Simulation parameters for both simulation suites

Suite	Box size h^{-1} Mpc	Cell size h^{-1} kpc	M_{cold}^a $(\Omega_c + \Omega_b) h^{-1} h^{-1} M_{\odot}$	N_{steps}	M_{min}^b $\Omega_0 h^{-1} M_{\odot}$	f^c
high res	75	65	2.09×10^9	200	3.4×10^{11}	0.078
low res	300	390	1.34×10^{11}	150	7.3×10^{13}	0.043

^a For models with massive neutrinos, $M_{\text{hot}} = M_{\text{cold}}\Omega_{\nu}/2(\Omega_c + \Omega_b)$.

^b Halo detection cutoff, from the restriction that halos must be larger than the grid size.

^c Fractional error in mass for the smallest halos identifiable.

ters in all the models in a given suite. Note that the models do have different power spectra and fluctuation growth rates, so distributions can differ for objects with different masses.

3 DARK MATTER HALOS

3.1 Halo finding algorithm

Most comparisons of dissipationless simulations with observational data require identification of dark matter halos. We locate halos in a similar manner to the spherical overdensity algorithm of KNP97, with some of the limits removed:

(i) We define candidate halos as the centers of all density maxima containing an overdensity greater than $\delta \equiv \delta\rho/\Omega_0\rho_c = 50$. A density maximum is defined as a cell whose density is greater than its six Cartesian neighbors. Just in case there are other halos hiding in those six neighbors, we also consider each of them to be candidates. Note that the finite grid size (as in all other grid-based halo finders, such as DENMAX, Gelb & Bertschinger 1994) will introduce a minimum separation between halos, which may cause small halos to be missed, which in turn will require a mass cut.

(ii) Each candidate halo then has the location of its center set iteratively to the center of mass of all the particles inside a sphere of diameter equal to the resolution ($65 h^{-1}$ kpc in our high resolution case). Halos are expected to have a minimum size of the order of the grid size, so this procedure moves the candidate halo to the peak of the density maximum. Of course, since we have defined more than one candidate for each detected maximum, some candidates will converge on the same halo. The smaller mass object in a given pair is removed if the distance between the centers of mass is less than half the grid spacing.

(iii) We perform a central overdensity cut. All halos that don't enclose a mean overdensity sufficient for virialization according to the spherical collapse model at the end of the center-of-mass detection phase are presumed not to be virialized objects and are discarded. Typically, this reduces the number of halos by a factor of 2–3, though the number is model dependent.

(iv) We now estimate at what radius the mean enclosed overdensity $\delta \equiv \delta\rho/\Omega_0\rho_c$ falls to δ_{vir} , the virial radius of the halo in spherical infall models.⁸ For each halo, we count the number of particles within five radii up to five grid cells ($325 h^{-1}$ kpc in this case) away from the center, convert that to

density, and interpolate the radius at which $\delta = \delta_{\text{vir}}$ (r_{vir}) using power-law cubic splines. If five radii is not large enough to enclose r_{vir} , we search five more radii, each twice as long as the original radii. This is repeated until we enclose r_{vir} .

(v) We define the mass of the halo as the mass enclosed in r_{vir} . The velocity is the mean velocity of all the particles within r_{vir} .

(vi) In general, the largest halos in a high resolution run contain much resolved but bound substructure. Because we search for the $\delta = \delta_{\text{vir}}$ radius, we detect the same regions of space dozens of times for the largest halos. This is unphysical, and the mass function is severely skewed. To fix this problem, the halos are searched in reverse order by mass to see if they enclose the centers of any smaller halos. If so, the smaller halo is thrown away. Note that the ordering is important because three-body intersections would be non-deterministic otherwise, and throwing away halos that only intersect is too stringent.

One limitation of this algorithm is that it presumes all halos are spherically symmetric, which is demonstrably untrue. But the effect on the mass function is *random*, rather than systematic, and finding the halos with an algorithm generalized to *ellipsoidal* distributions does not change the mass function significantly, even though it changes the parameters of individual halos. Because the halos have finite size, one cannot perform mass-weighted correlation function analyses, for distances less than the largest halo radius (about 2–3 h^{-1} Mpc in radius, typically).

The other limitation is the use of the density grid to identify halo candidates. If one considers a worst-case identification where a large number of particles all collect in one corner of a grid cell, in order to guarantee that all nearby halos are identified, one must draw a sphere which encloses the *entire* cell, of radius

$$r_{\text{min}} = \sqrt{3}L/N_{\text{g}}^{1/3}, \quad (7)$$

where L is the length of one side of the computational volume and N_{g} is the number of grid cells. If halos happen to be bigger than that, then the last step of the halo catalog generator makes it unimportant that we couldn't see nearby structure. Fortunately, halo extent is trivially related to halo mass because we have defined both where the mean overdensity is $\delta = \delta_{\text{vir}}$.

The most numerically sound way around the grid effect would be to estimate local density by finding the distance r to the N th nearest neighbor and setting the density to $3N/4\pi r^3$. On a distributed-memory supercomputer, this is exceedingly expensive, because the N th nearest particle may be on another processor (and it is *not* possible to guarantee it is on a *neighboring* processor), requiring a vast amount

⁸ Note that our definition of δ_{vir} is related to Eke, Cole, & Frenk (1996) by $1 + \delta_{\text{vir}} = \Delta_{\text{ECF}}/\Omega$. Our choice is appropriate for the density field calculations in an N -body code.

of communication to search. But, even with our nonoptimal density determined from the density grid (and hence, very noisy in low-density regions), we still have over three orders of magnitude dynamic range in mass for the high-resolution runs, which is sufficient for our purposes.

3.2 The effect of mass resolution

To what extent should you, the reader, trust the mass functions presented in this paper? To answer that, one must consider several effects. A typical feature in a mass function is that the large-mass end becomes ‘wiggly,’ usually blamed on the scarcity of high mass halos combined with cosmic variance. There is a related effect at somewhat smaller masses, since very large halos tend to have somewhat massive companions. For example, in most models in our high resolution suite, $5 \times 10^{13} h^{-1} M_{\odot}$ objects are fairly rare, but it is common to see them as companions for $10^{15} h^{-1} M_{\odot}$ objects. So, the wiggles may propagate down the mass function, and cosmic variance may have a significant effect on more than just the highest mass scales.

Cosmic variance fortunately leaves a signature, in that the mass function is not smooth at high masses. But, it is quite important to figure out the limiting factors at low mass, where typical mass functions are quite smooth. What limits accuracy here are the effects of finite sized grids and finite numbers of particles.

The effect of the finite sized grid was discussed above, and one must merely translate the minimum radius of a halo r_{\min} to a minimum mass. Since the halo radius and mass are defined as enclosing a mean overdensity of δ_{vir} , the mass M_{vir} of a halo of radius r_{vir} is

$$M_{\text{vir}} = (1 + \delta_{\text{vir}}) \frac{4\pi}{3} \Omega_0 \rho_c r_{\text{vir}}^3. \quad (8)$$

So, a *very* conservative mass cut is

$$M_{\min} = (1 + \delta_{\text{vir}}) \frac{4\pi}{3} \Omega_0 \rho_c \frac{(L\sqrt{3})^3}{N_g}. \quad (9)$$

Plugging in values for the high resolution suite, the mass cut is $3.4 \times 10^{11} \Omega_0 h^{-1} M_{\odot}$. For simplicity, we make the same mass cut on all models, corresponding to $\Omega_0 = 1$.

The effect of a finite number of particles is expressed in the significance of the detection of a halo. Because halo boundaries are defined where the mean overdensity δ is δ_{vir} and the mass of a particle is

$$M_p = \Omega_0 \rho_c \frac{L^3}{N_p}, \quad (10)$$

where N_p is the number of particles in the simulation, the number of particles inside a halo of mass M_{vir} in a simulation box of size L is

$$N_{\text{vir}} = \frac{M_{\text{vir}} N_p}{\Omega_0 \rho_c L^3}. \quad (11)$$

For counting N particles within r , the random variation in number is $\sigma = \sqrt{N}$. Let us suppose there are N_h halos above a given mass, and we wish to detect them all. We presume that counting halos is a Gaussian process and state that the n -sigma uncertainty in the detection of the halos corresponds to incorrectly detecting or missing a fraction $\text{erfc}(n/\sqrt{2})$ of the halos. We require detection of all halos, so the fraction missed should be less than $1/\rho L^3$, where ρ is

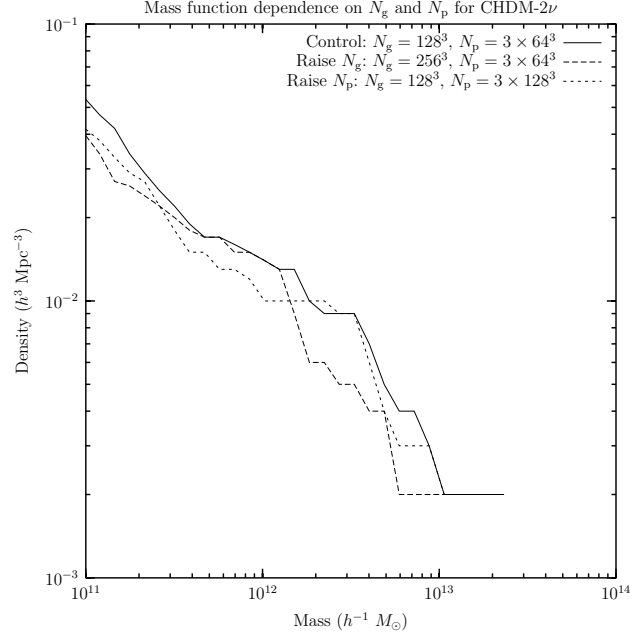


Figure 5. Effect of raising the number of particles or the number of grid cells by a factor of 8 in a very small CHDM-2 ν $10 h^{-1}$ Mpc simulation with $N_g = 128^3$ and $N_p = 3 \times 64^3$. The mass functions are not significantly different. A somewhat low mass cutoff of $10^{11} h^{-1} M_{\odot}$ has been applied. The high resolution suite has a linear cell size that is slightly smaller than the $N_g = 128^3$ runs shown in this figure.

the number density of halos above the mass cutoff, and L^3 is the volume of the simulation box where halos are identified. Inverting, we need detections of $\sqrt{2} \text{erfc}^{-1}(1/\rho L^3)$ sigma. Presuming a *high* density estimate for masses of $10^{11} h^{-1} M_{\odot}$ of $1 h^3 \text{Mpc}^{-3}$, we need to have at least 4.7σ detections of all halos. This means every halo must contain at least 23 particles, or more generally,

$$N_{\min} = 2 \left[\text{erfc}^{-1} \left(\frac{1}{\rho L^3} \right) \right]^2 \quad (12)$$

for the rather liberal restriction that we only require detection of the halo. Requiring a 10 per cent or less $1\text{-}\sigma$ error in mass is a more stringent requirement, and every halo must have at least 100 particles, since mass is determined by counting particles within several radii. So, if one requires a fractional error of f for a minimum halo mass of M_{\min} , one needs at least

$$N_p = \frac{\Omega_0 \rho_c L^3}{f^2 M_{\min}} \quad (13)$$

particles in the simulation. The parameters used, and the effective f they allow, are shown in table 2. Figure 5 shows that, with grid sizes and mean interparticle spacings of the order of those used in our suite, the effect of lowering either the grid size or the mean interparticle spacing by a factor of two does not significantly affect the mass function. For this test, we raised the threshold for halo candidate identification from $\delta = 50$ in one cell to $\delta = 70$ because one isolated cold particle in the high N_g case can give $\delta = 51.2$.

To explicitly test the effect of grid sizes on our mass functions, we ran five small simulations of the CHDM-2 ν

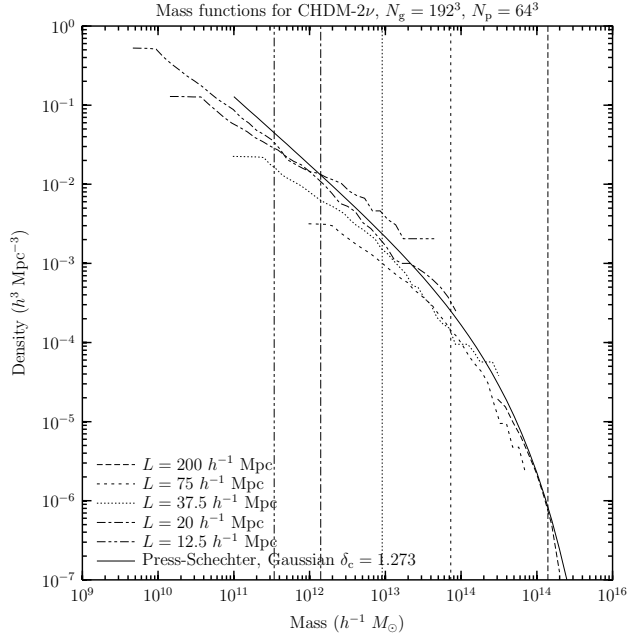


Figure 6. Effect of grid size on mass functions. The curves represent very small simulations of various sizes. Press-Schechter was tuned only to the largest box run, to get the clusters right. Note that the envelope mirrors the Press-Schechter curve reasonably well, but each individual mass function has a power-law index that is too shallow. Mass functions are limited at the large-mass end by statistics – one simply runs out of enough space to create objects in – and on the small-mass end by some fraction of the halos becoming as small as two grid cells, which means it is not guaranteed that the halo can be resolved from its neighbors, particularly if they are also small halos. The vertical lines represent the lower limit in mass for each run, above which all halos can be detected.

model with $N_g = 192^3$ grid cells and $N_p = 3 \times 64^3$ particles, with various-sized boxes. Though these simulations are too small to generate meaningful mass functions on their own, collectively, their upper envelope does match the Press-Schechter formula reasonably well, for $\delta_{c,g} = 1.2$ with a Gaussian filter. Figure 6 shows the five different mass functions. Also shown are lower mass cuts, determined for every model using equation (9). Above the mass cutoffs, every mass function agrees with the one for the next smaller box. Well below, the mass function slopes are not steep enough, but they agree with the neighboring curves for significant distances below the mass cuts, so it may be reasonable to extrapolate the mass function further. Every halo detected by the halo finder is represented in the figure, and where the lower mass cuts should be is indicated by vertical lines. Note that it is not possible to fit the envelope with a more standard $\delta_{c,g} = 1.5$ or $\delta_{c,t} = 1.68$ Press-Schechter curve. This test could conceivably overproduce clusters because of the extremely poor force and mass resolutions in the largest volume run – a cell width is about the size of an Abell radius. This δ_c result does persist for much larger simulations, as discussed below.

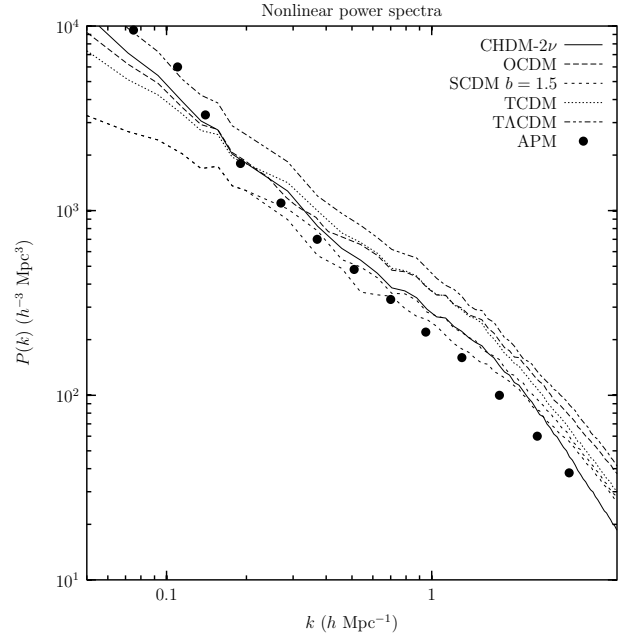


Figure 7. Nonlinear real-space dark matter power spectra, compared to the APM real-space galaxy power spectrum (Baugh & Efstathiou 1994) of galaxy number-count fluctuations. The simulation power spectra shown here are a composite of the high and low resolution suites, where data from a model’s high resolution run is used at large k and low resolution data is used at small k . Two different high resolution runs of the SCDM case are shown as a guide to how large cosmic variance is. The power in the second SCDM realization is 20–30 per cent lower than that in the first realization for $0.3 \lesssim k \lesssim 1 h \text{ Mpc}^{-1}$. The APM data are presumably biased with respect to the matter power spectrum, and yet the OCDM, TCDM, and TACDM cases require very large scale-dependent antibiasing to be consistent with the APM data, with $b^2 \sim 0.3$ for OCDM and TCDM and $b^2 \sim 0.5$ for TACDM at $k \sim 1 h \text{ Mpc}^{-1}$. Note that APM is known to miss galaxies in clustered regions, which would give a low power spectrum on scales of $k \gtrsim 1 h \text{ Mpc}^{-1}$ (Zabludoff, private communication).

4 RESULTS

The connection between simulations and observations is still fairly uncertain, and the least well determined portion of it is the galaxy identification procedure. It is therefore helpful to do as much analysis as one can on the *matter*, rather than the halos. Currently, only bulk flow motions (Kolatt & Dekel 1997) provide a meaningful *matter* power spectrum, but the large smoothing required means that the comparison is best made to the linear power spectrum (see figure 4). When looking at *galaxies*, one can only place bounds, based for example on the expectation that galaxies are more clustered than the dark matter. Figure 7 shows nonlinear real-space dark matter power spectra for all our models, compared to the APM real-space galaxy power spectrum (Baugh & Efstathiou 1994). The OCDM model requires significant antibiasing and the Λ CDM model requires even more. There is no evidence for such strong antibiasing, and it is very difficult to explain physically, especially on such large scales (cf. Yepes et al. 1997; Kauffmann, Nusser, & Steinmetz 1997). Additional arguments against strongly scale-dependent antibiasing are given in KPH96.

The process of galaxy formation is not well understood, so one could argue that perhaps there *is* some mechanism that would give us strong antibiasing. In order to probe that, we created an extreme model for galaxy formation designed to produce as much antibias as possible (cf. KPH96). Everywhere in the density grid, if there is more than $2.1 \times 10^9 h^{-1} M_\odot$ in a grid cell, we presume one galaxy forms there. That mass corresponds to slightly more than the mass due to one isolated particle in the high-resolution SCDM and TCDM simulations (which have the most massive particles in the suite). Such a limit is necessary to prevent placing excess power in the voids due to vestiges of the initial grid there.⁹ This is a highly unreasonable model for galaxy formation, as it says that the density of $\gtrsim 2 \times 10^{11} h^{-1} M_\odot$ galaxies in the core of the Coma cluster should be the same as in the local group, and this is clearly ruled out observationally. However, even though there is significant antibias on small scales, it is only visible at scales smaller than about $k = 1 h \text{ Mpc}^{-1}$ (see figure 8), whereas antibiasing is needed on scales larger than that in order for OCDM or TACDM to be consistent with the APM power spectrum. Note that a way out of the antibiasing requirement is to note that the APM survey is incomplete in clustered regions, which will raise the ‘true’ power spectrum above the APM measurement (Zabludoff, private communication).

The APM power spectrum is not the only power spectrum that has been measured. However, to compare to other measurements, it is usually required to calculate model redshift space power spectra. Going to redshift space significantly reduces power on scales of interest, since typical dispersion velocities of 1000–2000 km s^{-1} in clusters correspond to a scatter of 10–20 $h^{-1} \text{ Mpc}$ in distance. In performing this operation on particles, the power should be viewed as a lower bound, because there may be significant velocity bias (Carlberg, Couchman, & Thomas 1990; Summers, Davis, & Evrard 1995), meaning the power perhaps shouldn’t be suppressed *quite* as much, and galaxy formation will further raise the power. Figure 9 shows the models’ redshift space power spectra, compared to the combined CfA2 and SSRS2 redshift space power spectrum (da Costa et al. 1994). Given our choices of model normalization and cosmological parameters, the TACDM matter power spectrum is nicely consistent with the observed galaxy power spectrum, but that leaves *no* room for galaxy formation or velocity bias effects. As for the real-space nonlinear power spectrum comparison (figure 7), this requires significant antibiasing for TACDM on scales of 0.3–1 $h \text{ Mpc}^{-1}$. Note that under-sampling the velocity field will miss the large velocities by making the halos physically larger, so it does not make sense to perform redshift space comparisons on the large volume suite.

⁹ One can see that there must be *some* particles there by calculating how long it would take to evacuate a void. We see voids in many of the simulations as big as they can be given the constraints of the simulation parameters – half the box size, or $\sim 35 h^{-1} \text{ Mpc}$ in diameter. If particles were moving as fast as 1000 km s^{-1} away from the center of the void, it would take about 17 Gyr for them to completely leave a $35 h^{-1} \text{ Mpc}$ diameter void, which is more than the age of the universe for all models considered here. Particles in voids almost never move nearly that fast, particularly those near the center of the void.

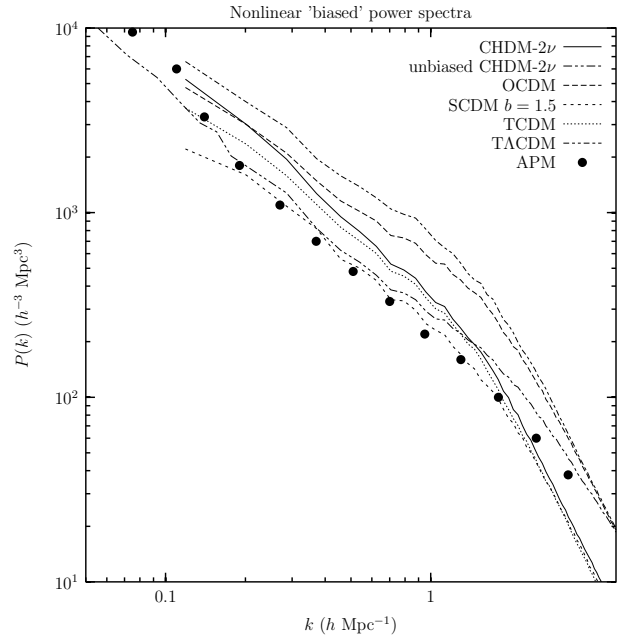


Figure 8. Nonlinear power spectra, presuming an extreme scale-dependent biasing scheme. The density field has been set to ‘on’ at any cell containing mass exceeding the largest particle mass in the $75 h^{-1} \text{ Mpc}$ suite, $2.1 \times 10^9 h^{-1} M_\odot$, and ‘off’ everywhere else. That mass cut is most likely lower than anything that could make it into the CfA2 or APM catalogs, except if one assumes an impossibly small mass-to-light ratio. The result of such a bizarre galaxy identification scheme is a bias on large scales, due to clearing out the void regions, and an antibias on small scales, due to removing the high peaks in density. We do comparisons with the high resolution suite because the low resolution suite particle mass is too high.

Most observational programs measure halo dependent quantities, such as number counts of galaxies, correlation studies, and so forth. So, we report results that are dependent upon halo identification, with the caveat that a physically based galaxy identification algorithm does not yet exist, especially for dissipationless simulations.

The simplest measurement we can make on the halos is counting the number density of bound objects as a function of mass. Such ‘mass functions’ and close relatives such as the X-ray temperature function (as in Eke, Cole, & Frenk 1996, for example) are often estimated from the Press-Schechter approximation instead of from simulations. Though it has been checked against scale-free simulations (Efstathiou et al. 1988; Bond et al. 1991; Lacey & Cole 1994) and against specific SCDM, Λ CDM and CHDM models (Carlberg & Couchman 1989; Jain & Bertschinger 1994; Klypin et al. 1995; Walter & Klypin 1996; Bond & Myers 1996), previous studies have focused only on a narrow range of masses, typically at the cluster scale. With our large simulations, we can check the approximation over four orders of magnitude in mass. The Press-Schechter formula we use is Klypin et al. (1995), equations (1–2), evaluated at $z = 0$:

$$N(> M) = \sqrt{\frac{2}{\pi}} \frac{\delta_c}{\alpha_m} \int_r^\infty \frac{\epsilon(r')}{\sigma^3(r')} \exp\left[\frac{-\delta_c^2}{2\sigma^2(r')}\right] \frac{dr'}{r'^3}, \quad (14)$$

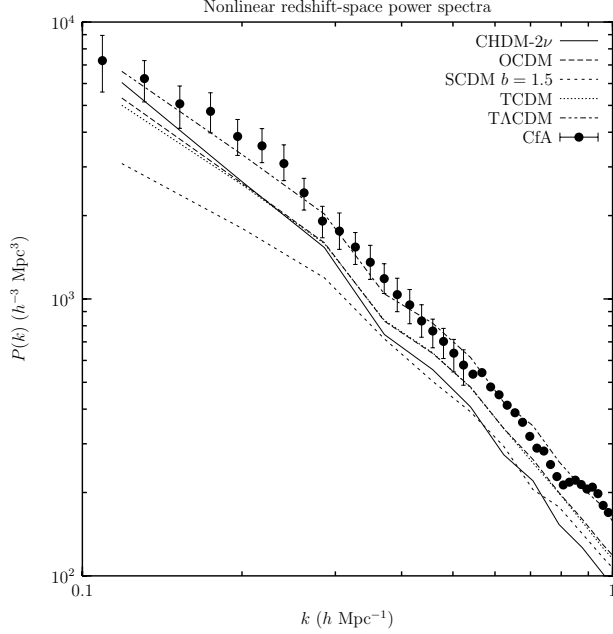


Figure 9. Redshift space power spectrum, compared to the combined CFA2 and SSRS2 redshift space power spectrum (da Costa et al. 1994). Notice that, while Λ CDM is a good match to this power spectrum, that leaves no room for galaxy formation or velocity bias.

Table 3. Press-Schechter fits to simulation mass functions

Model	$\delta_{c,t}$	$\delta_{c,g}$
CHDM- 2ν	1.571	1.273
OCDM	1.693	1.293
SCDM $b = 1.5$	1.672	1.236
TCDM	1.630	1.252
TACDM	1.732	1.355

$\delta_{c,t}$ and $\delta_{c,g}$ have been chosen to get the same number density of clusters with $M > 5.5 \times 10^{14} h^{-1} M_{\odot}$ as the large-volume simulation, for each model.

where

$$\epsilon(r) = \frac{1}{2\pi} \int_0^{\infty} k^3 P(k) W(kr) \frac{dW(kr)}{d(kr)} dk, \quad (15)$$

$$\sigma^2(r) = \frac{1}{2\pi^2} \int_0^{\infty} k^2 P(k) W^2(kr) dk, \quad (16)$$

$$W(x) = \begin{cases} \frac{3}{x^3} [\sin(x) - x \cos(x)] & \text{tophat} \\ e^{-x^2/2} & \text{Gaussian} \end{cases}, \quad (17)$$

$$r = \left(\frac{M}{\alpha_m \rho_c \Omega_0} \right)^{\frac{1}{3}} \quad (18)$$

and α_m is $4\pi/3$ for a tophat window function, and $(2\pi)^{3/2}$ for a Gaussian window function.

Figure 10 shows the cumulative mass functions estimated from both suites of simulations, and

table 3 shows the Press-Schechter parameters used in that figure. Note that in the overlapping region, the two sets of simulation mass functions are consistent, and the high

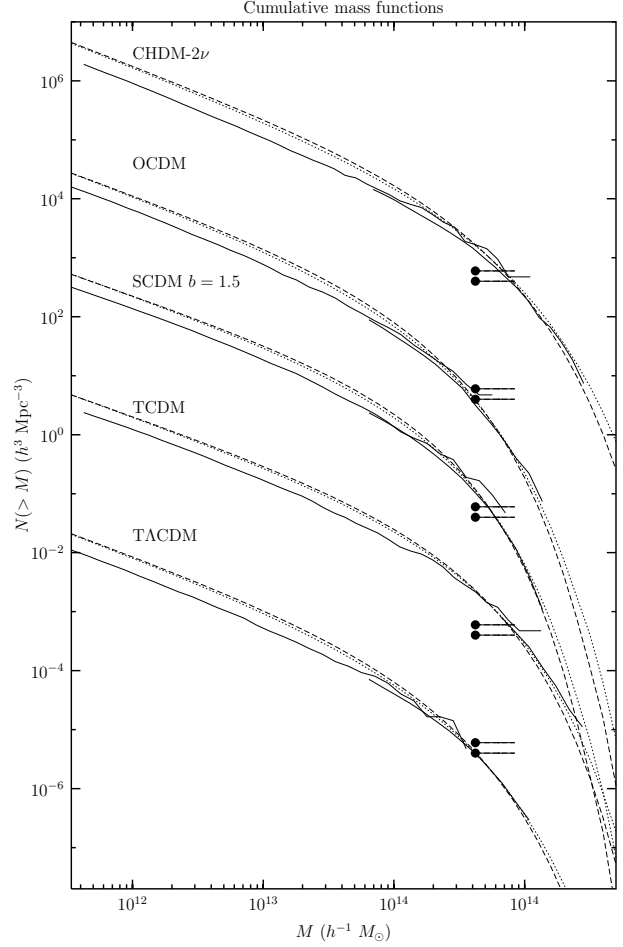


Figure 10. Cumulative halo mass functions, with Press-Schechter fits. In each panel, the relevant mass functions estimated from the two simulation suites is shown by the full curves. Small mass cuts have been applied at $M = 3.4 \times 10^{11} h^{-1} M_{\odot}$ and $2.2 \times 10^{13} h^{-1} M_{\odot}$, for the large and small volume simulations, respectively. Each panel also shows Gaussian (dashed curves) and tophat (dotted curves) Press-Schechter mass functions, normalized to agree with the large-volume simulations at $5.5 \times 10^{14} h^{-1} M_{\odot}$. The values of $\delta_{c,t}$ and $\delta_{c,g}$ used are given in table 3. The data points correspond to the observations of BGGM93 and WEF93, as in figure 1. Each model's data have been offset vertically by a factor of 10^{2j} to separate the different models from each other, and the cluster constraints have been replicated for each model.

resolution results are a significant factor of 1.5–2 below the Press-Schechter estimates for all models at the intermediate mass of $10^{13} h^{-1} M_{\odot}$ and below. As figure 11 shows, the intermediate and low mass discrepancy *cannot* be fixed by adjusting the value of δ_c , particularly at a mass of $\sim 5 \times 10^{12} h^{-1} M_{\odot}$, where the curves cross. Our values of $\delta_{c,t}$ and $\delta_{c,g}$ are consistent with Borgani et al. (1997b), and the tophat case is consistent with the spherical collapse model.

Our two low- Ω_0 models produce fewer clusters in simulations than the other models (figure 10). If X-ray temperature cluster masses are correct, this presents no problem for those models. However, if gravitational lensing cluster masses are correct, they require fixing by using less tilt or a smaller H_0 . The former is more urgent, because it

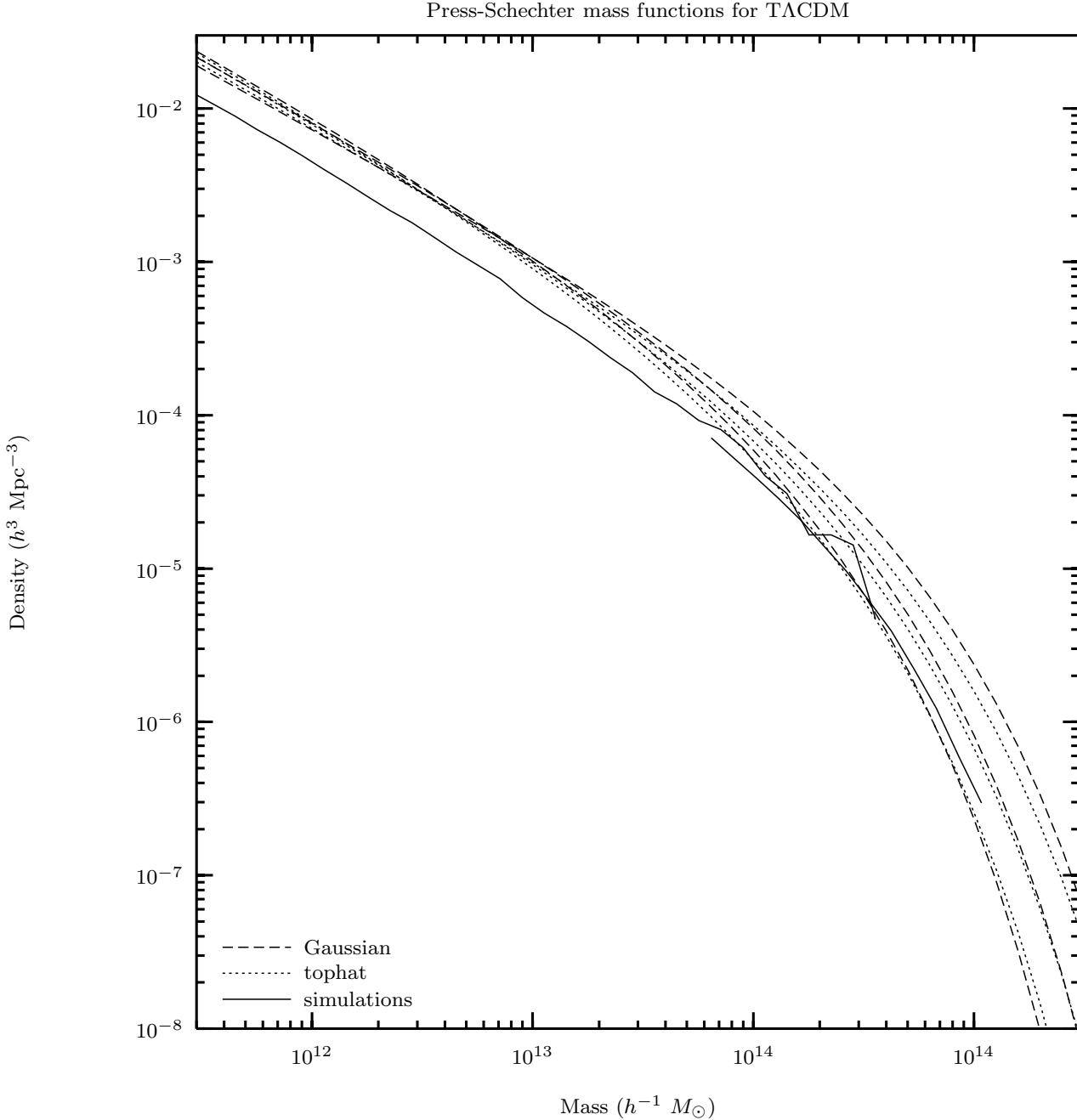


Figure 11. Press-Schechter mass functions for TACDM. The high and low density TACDM mass functions from simulations are shown in the solid curves. From top to bottom at $M = 10^{15} h^{-1} M_{\odot}$, the dashed curves show Press-Schechter mass functions with Gaussian filters for $\delta_{c,g} = 1.0, 1.2,$ and 1.4 , and the dotted curves show tophat filters for $\delta_{c,t} = 1.4, 1.6,$ and 1.8 . Press-Schechter mass functions can be made to agree with our simulations for masses above about $5 \times 10^{13} h^{-1} M_{\odot}$, but not for masses smaller than that.

helps lessen the disagreement with high-multipole cosmic microwave background measurements (figure 2), as a weaker tilt would raise the first Doppler peak. If X-ray temperature masses are correct, TCDM and CHDM- 2ν produce too many clusters. This can be fixed most reasonably by raising H_0 , as both models use values that are on the low side of observations, and Hipparcos has greatly weakened the age constraint.

The statements above all take the normalizations we

have assumed as fixed constraints. Alternatively, we could turn the problem around and use the clusters to determine normalizations and tilts, with H_0 (and Ω_0 and Ω_{Λ}) as a given. This is explored further in Gross et al. (1997).

It would be desirable to compare halo-dependent results to actual data. One would now like to investigate statistics such as correlation functions, void probability functions (Ghigna et al. 1997), shape statistics (Davé et al. 1997), and other sophisticated statistics. However, to compare to obser-

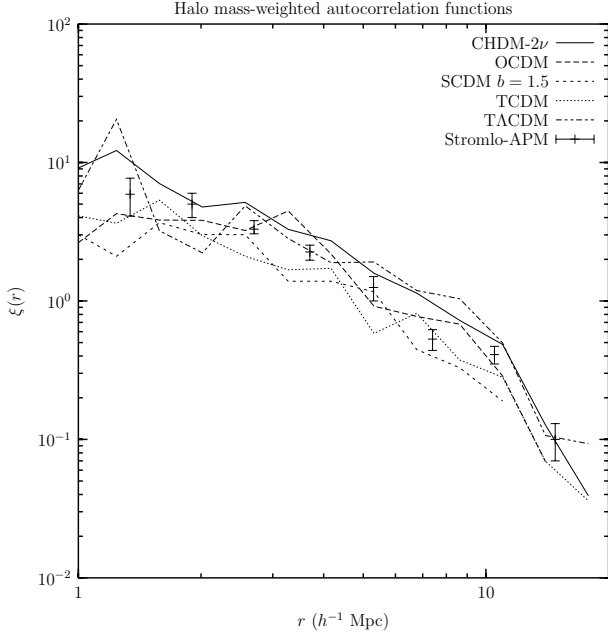


Figure 12. Halo mass-weighted correlation function. Only halos with mass above $3 \times 10^{11} h^{-1} M_{\odot}$ are included, and all pairs are weighted by the product of the two masses. Such a weighting is a simple countermeasure for the overmerging problem. The error bars are the Stromlo-APM autocorrelation function (Loveday et al. 1995).

vations, we need to know how many galaxies form in each halo. Previous studies (KNP97; Nolthenius, Klypin, & Primack 1997; Ghigna et al. 1997, for example) have used ad hoc ‘breakup’ prescriptions to populate halos with galaxies. We have developed semianalytic models of galaxy formation (Somerville 1997, based in part on Kauffmann & White 1993) and used them to populate the simulation halos with galaxies. This is the topic of subsequent work, so we do not attempt to identify galaxies here.

For certain statistics, one can partially compensate for the effect of overmerging by *mass weighting*. That approach is less than ideal because it does not restore the small-scale *spatial* information lost in the overmerging process. Mass weighting is equivalent to presuming a halo contains a number of galaxies proportional to its mass, and putting all the galaxies at the center of the halo. In effect, this clears out regions of space around the largest halos’ centers, equal to their radii, and therefore loses information on scales smaller than the largest halo radius (typically $2\text{--}3 h^{-1} \text{Mpc}$). Since very massive halos are rare objects for physically interesting cosmological models, all mass weighted statistics must be unduly influenced by small-number statistical noise.

We calculate the mass-weighted autocorrelation function for the high resolution runs, and the results are shown in figure 12. In this figure, a halo mass cut of $M = 3 \times 10^{11} h^{-1} M_{\odot}$ was used, although the mass weighting makes it insensitive to the mass cut. The mass weighting creates a spread in the correlation values large enough to prevent the test from discriminating among models. To within the spread visible in figure 12, all models are roughly consistent with the Stromlo-APM autocorrelation function (Loveday

et al. 1995). However, there are a few trends visible in the figure. SCDM and TCDM are systematically lower in amplitude than the other models, but the effect is not very significant given the spread. It is interesting that these models were not the highest normalized models in the suite.

5 CONCLUSIONS

We have run two suites of simulations with 57 million cold particles in boxes of 75 and $300 h^{-1} \text{Mpc}$, with the goal of studying interesting variants of the CDM family of cosmological models. In this paper, we have made preliminary comparisons of the $z = 0$ simulation outputs to data for all models. More detailed comparisons with observations require assumptions about galaxy formation and will be treated in subsequent work. Subject to the usual caveats about the uncertainty of galaxy formation, we reach the following conclusions:

(i) We generalize the results of KPH96 to a different Λ CDM model. The APM real-space power spectrum (Baugh & Efstathiou 1994) compared to the TACDM matter power spectrum requires large antibias of $b^2 \equiv P_{\text{gal}}/P_{\text{dm}} \sim 0.3$ at $k = 1 h \text{Mpc}^{-1}$. OCDM is only slightly better, and it still requires a strong antibias of $b^2 \sim 0.5$. All other models require a weaker antibias at that scale. Designing an excessively antibiased galaxy formation scenario doesn’t help at the $r \sim 6 h^{-1} \text{Mpc}$ scale, as it is bigger than any individual dark matter halo. To get strong antibiasing on such a scale, there would need to be much dark matter where there aren’t many galaxies forming.

(ii) The TACDM dark matter redshift space power spectrum agrees very well with the redshift space galaxy power spectrum from CfA2+SSRS2 (da Costa et al. 1994). This leaves no room for bias expected in normal galaxy formation, or for velocity biases. For comparison, OCDM and TCDM each have room for a modest bias of $b^2 \sim 1.2$ at $k = 0.5 h \text{Mpc}^{-1}$, and CHDM-2 ν and SCDM each need $b^2 \sim 1.5$.

(iii) All models considered here are consistent with the Stromlo-APM real-space correlation function (Loveday et al. 1995) on scales of $2\text{--}20 h^{-1} \text{Mpc}$, largely due to a large spread in the model estimates of the correlation function because of mass weighting and small-number statistics for large mass objects.

(iv) The Press-Schechter approximation fits the abundance of cluster-mass halos very well, with top-hat $\delta_{c,t} = 1.63\text{--}1.73$ and Gaussian $\delta_{c,g} = 1.22\text{--}1.36$. But, it overpredicts the density of galaxy and small group mass objects by a factor of ~ 2 , only weakly dependent on cosmology, and very weakly dependent on δ_c . On mass scales of $\sim 5 \times 10^{12} h^{-1} M_{\odot}$, it is not possible to compensate for the discrepancy by adjusting δ_c within reasonable bounds.

6 ACKNOWLEDGEMENTS

MAKG and JRP were supported by NSF and NASA grants at UCSC, RSS was supported by a GAANN fellowship, and JH and AK were supported by NSF and NASA grants at NMSU. The simulations were run on the IBM SP2 at the Cornell Theory Center, Cornell University, Ithaca, NY, USA

and computer time for analysis was provided by Sandra Faber and the WF/PC project.

REFERENCES

- Bardeen J. M., Bond J. R., Kaiser N., Szalay A. S., 1986, *ApJ*, 304, 15 (BBKS)
- Bartlett J. G., Blanchard A., Silk J., Turner M. S., 1995, *Science*, 267, 980
- Baugh C. M., Efstathiou G., 1994, *MNRAS*, 267, 323
- Bernardeau F., Juszkiewicz R., Dekel A., Bouchet F., 1995, *MNRAS*, 274, 20
- Binggeli B., 1982, *A&A*, 107, 338
- Biviano A., Girardi M., Giuricin G., Mardirossian F., Mezzetti M., 1993, *ApJ*, 411, L13 (BGMM93)
- Blumenthal G. R., Faber S. M., Primack J. R., Rees M. J., 1984, *Nat*, 517
- Bond J. R., Cole S., Efstathiou G., Kaiser N., 1991, *ApJ*, 379, 440
- Bond J. R., Myers S. T., 1996, *ApJS*, 103, 41
- Borgani S., Gardini A., Girardi M., Gottlöber S., 1997a, *New Astronomy*, 2, 119
- Borgani S. et al., 1997b, *New Astronomy*, 1, 299
- Bunn E. F., White M., 1997, *ApJ*, 480, 6
- Carlberg R. G., Couchman H. M. P., 1989, *ApJ*, 340, 47
- Carlberg R. G., Couchman H. M. P., Thomas P. A., 1990, *ApJ*, 352, L29
- Chaboyer B., Demarque P., Kernan P. J., Krauss L. M., 1997, preprint, astro-ph/9706128
- Couchman H. M. P., 1991, *ApJ*, 368, L23
- da Costa L. N., Vogeley M. S., Geller M. J., Huchra J. P., Park C., 1994, *ApJ*, 437, L1
- Davé R., Hellinger D., Primack J. R., Nolthenius R., Klypin A., 1997, *MNRAS*, 284, 607
- Davis M., Efstathiou G., Frenk C. S., White S. D. M., 1985, *ApJ*, 292, 371
- Dekel A. et al., 1997, in preparation
- Dekel A., Rees M. J., 1994, *ApJ*, 422, L1
- Efstathiou G., Frenk C. S., White S. D. M., Davis M., 1988, *MNRAS*, 235, 715
- Eke V. R., Cole S., Frenk C. S., 1996, *MNRAS*, 282, 263
- Gelb J. M., Bertschinger E., 1994, *ApJ*, 436, 467
- Ghigna S., Borgani S., Tucci M., Bonometto S. A., Klypin A., Primack J. R., 1997, *ApJ*, 479, 580
- Górski K. M., Banday A. J., Bennett C. L., Hinshaw G., Kogut A., Smoot G. F., Wright E. L., 1996, *ApJ*, 464, L11
- Gratton R. G., Pecci F. F., Carretta E., Clementini G., Corsi C. E., Lattanzi M., 1997, preprint, astro-ph/9704150
- Gross M. A. K., 1997, Ph.D. thesis, UCSC
- Gross M. A. K., Somerville R. S., Primack J. R., Borgani S., Girardi M., 1997, submitted
- Henry J. P., Arnaud K. A., 1991, *ApJ*, 372, 410
- Hockney R. W., Eastwood J. W., 1988, *Computer Simulation Using Particles*. Institute of Physics Publishing, Philadelphia
- Hoffman Y., 1986, *ApJ*, 308, 493
- Holtzman J. A., 1989, *ApJS*, 71, 1
- Hu W., Sugiyama N., 1996, *ApJ*, 471, 542
- Hu W., White M., 1997, *ApJ*, 486, L1
- Jain B., Bertschinger E., 1994, *ApJ*, 431, 495
- Jenkins A. et al., 1996, preprint, astro-ph/9610206
- Kates R. E., Kotok E. V., Klypin A., 1991, *A&A*, 243, 295
- Kauffmann G., Nusser A., Steinmetz M., 1997, *MNRAS*, 286, 795
- Kauffmann G., White S. D. M., 1993, *MNRAS*, 261, 921
- Klypin A., Borgani S., Holtzman J., Primack J., 1995, *ApJ*, 444, 1
- Klypin A., Gottlöber S., Kravtsov A. V., 1997, preprint, astro-ph/9708191
- Klypin A., Holtzman J., Primack J., Regös E., 1993, *ApJ*, 416, 1
- Klypin A., Nolthenius R., Primack J., 1997, *ApJ*, 474, 533 (KNP97)
- Klypin A., Primack J., Holtzman J., 1996, *ApJ*, 466, 1 (KPH96)
- Kolatt T., Dekel A., 1997, *ApJ*, 479, 592
- Kravtsov A. V., Klypin A., Khokhlov A. M., 1997, *ApJS*, 111, 73
- Lacey C., Cole S., 1993, *MNRAS*, 262, 627
- Lacey C., Cole S., 1994, *MNRAS*, 271, 676
- Lahav O., Lilje P. B., Primack J. R., Rees M. J., 1991, *MNRAS*, 251, 128
- Landau L. D., Lifshitz E. M., 1976, *Mechanics* (3rd ed.). Pergamon, Oxford
- Liddle A. R., Lyth D. H., Roberts D., Viana P. T. P., 1996, *MNRAS*, 278, 644 (LLRV96)
- Lineweaver C. H., Barbosa D., 1997, preprint, astro-ph/9706077
- Loveday J., Maddox S. J., Efstathiou G., Petersen B. A., 1995, *ApJ*, 442, 457
- Miralda-Escudé J., Babul A., 1995, *ApJ*, 449, 18
- Misner C. W., Thorne K. S., Wheeler J. A., 1973, *Gravitation*. W. H. Freeman & Co., New York
- Monaco P., 1995, *ApJ*, 447, 23
- Netterfield C. B., Devlin N., Jarosik L., Page L., Wollack E. J., 1997, *ApJ*, 474, 47
- Nolthenius R., Klypin A., Primack J. R., 1997, *ApJ*, 480, 43
- Nusser A., Dekel A., 1993, *ApJ*, 405, 437
- Padmanabhan T., 1993, *Structure Formation in the Universe*. Cambridge Univ. Press, New York
- Pen U. L., 1996, astro-ph/9610147
- Platt S. R., Kovac J., Dragovan M., Petersen J. B., Ruhl J. E., 1997, *ApJ*, 475, L1
- Pogosyan D. Y., Starobinsky A. A., 1995, in Mucket J. P., Gottlöber S., Müller V., ed, *International Workshop on Large Scale Structure in the Universe*. World Scientific, River Edge, New Jersey
- Press W. H., Schechter P., 1974, *ApJ*, 187, 425
- Primack J. R., Holtzman J., Klypin A., Caldwell D. O., 1995, *Phys. Rev. Lett.*, 74, 2160
- Reid I. N., 1997, *AJ*, 114, 161
- Scott P. F. et al., 1996, *ApJ*, 461, L1
- Seljak U., Zaldarriaga M., 1996, *ApJ*, 469, 437
- Smith C. C., Klypin A., Gross M. A. K., Primack J. R., Holtzman J., 1997, *MNRAS*, submitted, astro-ph/9702099
- Smoot G. F. et al., 1992, *ApJ*, 396, L1
- Somerville R. S., 1997, Ph.D. thesis, UCSC
- Squires G., Kaiser N., Babul A., Fahlman G., Woods D., Neumann D. M., Böringer H., 1996, *ApJ*, 461, 572
- Squires G., Neumann D. M., Kaiser N., Arnaud M., Babul A., Böringer H., Fahlman G., Woods D., 1997, *apj*, 482, 482
- Summers F. J., Davis M., Evrard A. E., 1995, *ApJ*, 454, 1
- Tegmark M., 1996, *ApJ*, 464, L35
- Tytler D., Fan X., Burles S., 1996, *Nat*, 381, 207
- Viana P. T. P., Liddle A. R., 1996, *MNRAS*, 281, 323
- Walter C., Klypin A., 1996, *ApJ*, 462, 13
- White S. D. M., Efstathiou G., Frenk C. S., 1993, *MNRAS*, 262, 1023 (WEF93)
- Wu X. P., Fang L. Z., 1996, *ApJ*, 467, L45
- Wu X. P., Fang L. Z., 1997, *ApJ*, 483, 62
- Xu G., 1995, *ApJS*, 98, 355
- Yepes G., Kates R., Khokhlov A., Klypin A., 1997, *MNRAS*, 284, 235
- Zel'dovich Y. B., 1970, *A&A*, 5, 84

APPENDIX A: THE SPHERICAL COLLAPSE MODEL IN AN ARBITRARY COSMOLOGY AND AT ARBITRARY REDSHIFT

For the purposes of identifying halos in N -body simulations, we need a simple criterion to identify ‘virialized’ regions of space. The simplest such criterion is based upon the collapse of an isolated spherical overdensity in an otherwise uniform universe. This is *not* a correct assumption – halos regularly show axial ratios of $\mu_3/\mu_1 < 0.5$ and occasionally exhibit $\mu_3/\mu_1 < 0.3$, both in Abell clusters (Binggeli 1982) and in the simulations reported here. An ellipsoidal component, and especially a background shear field, always reduces the collapse time from the spherically symmetric case (Hoffman 1986; Jain & Bertschinger 1994; Monaco 1995). Such concerns are surely significant for individual halos, but the processes of collapse and virialization are not easily modelled because of inhomogeneous collapse, and the nonlocality implied by dependence on the shear field creates severe computational difficulties. So, for the purposes of identifying halos, we approximate the collapse as spherical. The spherical overdensity model has been generalized to open $\Omega_\Lambda = 0$ models by Lacey & Cole (1993) and to flat $\Omega_\Lambda + \Omega_0 = 1$ models by Eke, Cole, & Frenk (1996). The discussion here generalizes the model to any isotropic ‘big bang’ cosmology.

A1 From the initial time to maximum expansion

If one presumes an isolated spherical perturbation in an otherwise uniform universe, Birkhoff’s Theorem (Misner, Thorne, & Wheeler 1973, for example) applies, and the evolution of the perturbation is independent of the matter outside the spherical region. In particular, when considering the dynamics of the perturbation, we could pretend the background universe has the same mean density as the perturbation. So, if the object is destined to collapse, the evolution must be described by the Friedmann equation for a closed universe with the same cosmological constant,

$$\dot{b} = \pm H_0 \sqrt{\Omega_{\text{ta,eff}}/b + \Omega_\Lambda b^2 + \Omega_{\text{k,eff}}}, \quad (\text{A1})$$

where b is an effective scale factor defined so that $b = 1$ at maximum expansion, not to be confused with the scale factor a of the background universe. In this equation, we have defined the time variable to be the same as the background universe by requiring the same Hubble parameter today. That is encoded within the choice of critical density,

$$\Omega_{\text{ta,eff}} \equiv \frac{\rho(b=1)}{\rho_c} = \frac{8\pi G\rho(b=1)}{H_0^2}, \quad (\text{A2})$$

and the cosmological constant,

$$\Omega_\Lambda \equiv \frac{\Lambda}{3H_0}, \quad (\text{A3})$$

so the H_0 in equation (A4) is the same Hubble parameter as in the background universe. Because we have chosen a time variable determined by the background universe rather than the perturbation, the usual restriction that $\Omega_{\text{ta,eff}} + \Omega_\Lambda + \Omega_{\text{k,eff}} = 1$ does *not* apply. If it did, H_0 would be the Hubble parameter at maximum expansion, which is *not* today for any collapsed object.

Meanwhile, the background universe evolves with a different scale factor:

$$\dot{a} = H_0 a^{-1/2} \sqrt{\Omega_c + \Omega_\nu + \Omega_\Lambda a^3 + \Omega_{\text{k}} a}. \quad (\text{A4})$$

$\Omega_{\text{ta,eff}}$ is in general much higher than the background density parameter Ω_0 , and $\Omega_{\text{k,eff}}$ is negative for overdensities destined to collapse.¹⁰

Note that the Friedmann equation (equation A4) gives the derivative of b when b is given. To enforce the requirement that $b = 1$ at maximum expansion, we fix a relationship between $\Omega_{\text{ta,eff}}$ and $\Omega_{\text{k,eff}}$. Because $\dot{b} = 0$ at maximum expansion,

$$\Omega_{\text{k,eff}} = -(\Omega_{\text{ta,eff}} + \Omega_\Lambda). \quad (\text{A5})$$

When this happens, b can get no larger, or its derivative becomes imaginary, so it must turn around and afterward, we must use the negative sign for the derivative. This value of the derivative depends only on the value of b , so it must be the precise negative of the derivative taken when b had this particular value on the rising side of the curve. The time from $t = 0$ to maximum expansion is therefore

$$t_{\text{max}} = \int_0^1 \frac{db}{\dot{b}}. \quad (\text{A6})$$

Similarly, the time from maximum expansion to collapse is

$$t_{\text{coll}} - t_{\text{max}} = \int_1^0 \frac{db}{\dot{b}}, \quad (\text{A7})$$

Here, \dot{b} is the negative of the derivative in the previous equation, but the bounds of integration are also opposite. This means the two integrals have exactly the same values. That is,

$$t_{\text{coll}} = 2t_{\text{max}} \quad (\text{A8})$$

independent of cosmology.

For an arbitrary cosmological time, we wish to calculate the minimal perturbation that has collapsed (and presumably virialized) by that time. So, first we specify the time we wish to consider by the background universe’s expansion parameter a . That is a unique specification even for a closed universe, as long as the background universe has not started to recollapse yet. We convert that to an age by integrating and inverting the Friedmann equation:

$$t = \int_0^a \frac{da'}{\dot{a}'}. \quad (\text{A9})$$

Note that we are not requiring $a = 1$ ($z = 0$) at this time, though that is a reasonable special case. We require that collapse occur before this time. Since higher overdensities imply quicker collapse, setting the collapse time t_{coll} equal to t gives a lower bound for the overdensity.

We divide this time in two to find the time to maximum expansion, and then search for a value for $\Omega_{\text{ta,eff}}$ that satisfies

$$\frac{t}{2} = \int_0^1 \frac{db}{\dot{b}}, \quad (\text{A10})$$

where Ω_Λ is the same as for the background cosmology, and $\Omega_{\text{k,eff}} = -(\Omega_{\text{ta,eff}} + \Omega_\Lambda)$.

The resulting $\Omega_{\text{ta,eff}}$ is the mean density in the perturbation, divided by the critical density, at maximum expansion ($b = 1$; equation A2). The density perturbation, relative

¹⁰ Note that for $\Omega_\Lambda \neq 0$ models, the converse is not true; $\Omega_{\text{k,eff}} < 0$ is a necessary, but not sufficient, condition for collapse.

to the background density $\bar{\rho} = \Omega_0 \rho_{\text{crit},0}/a^3$ at the ‘final’ time a is therefore

$$1 + \delta_{\text{ta}} \equiv \frac{\rho_{\text{ta}}}{\bar{\rho}} = a^3 \frac{\Omega_{\text{ta,eff}}}{\Omega_0}. \quad (\text{A11})$$

A2 From maximum expansion to virialization

A detailed model of the process of collapse and virialization would be tremendously complicated, with dependences on the distribution and velocities of mass elements. Imposing spherical symmetry helps the situation, but the detailed dynamics are still dependent on the precise radial distribution of matter. But, the evolution of an overdensity is much more information than we really need, and simple energy arguments can give us the final configuration in terms of the initial. The tradeoff is that we don’t really know how long virialization takes, and a standard assumption is that it is roughly the collapse time, although density profiles are peaked in the center, and the center parts of halos collapse and virialize before the outer parts finish collapsing. As long as the density profile decreases monotonically from the center, no mass shell will cross another before the collapse time. We ignore shell crossings that must occur after collapse, during virialization. Of course, this is a poor model for mergers, which are the most likely physical mechanism for large halo collapse in a hierarchical universe, but we are presuming spherical symmetry anyway.

Following the derivation of Lahav et al. (1991), we consider the perturbation to be a spherically symmetric collection of particles, within some radius $r = lb$. The symmetry allows us to ignore the background cosmology and all particles outside r when examining the evolution of the portions internal to r . For an arbitrary test particle, the mass inside r is then

$$GM = \frac{1}{2} H_0^2 \Omega_{\text{ta,eff}} l^3 \quad (\text{A12})$$

(recall that $\Omega_{\text{ta,eff}}$ is the density at maximum expansion in units of the critical density). The force on this test particle is $F/m = -GM/r^2 = -H_0^2 \Omega_{\text{ta,eff}} l^3 / (2r^2) = -H_0^2 \Omega_{\text{ta,eff}} l / 2r^2$, which must be compared to the derivative of the Friedmann equation

$$\ddot{b} = H_0^2 \left[\Omega_\Lambda b - \frac{\Omega_{\text{ta,eff}}}{2b^2} \right], \quad (\text{A13})$$

which is seen to agree only if a cosmological constant term $H_0^2 \Omega_\Lambda r$ is added to the force. So, the potential energy per unit mass of a shell of radius R is the integral of this modified force, and

$$u = -\frac{1}{2} H_0^2 l^2 \left(\frac{\Omega_{\text{ta,eff}}}{b} + \Omega_\Lambda b^2 \right). \quad (\text{A14})$$

The total potential energy per unit mass inside b is the mass-weighted integral of u ,

$$\begin{aligned} U &= \frac{4\pi \rho_c \Omega_{\text{ta,eff}} \int_0^r R^2 u \, dR}{\frac{4\pi}{3} \rho_c \Omega_{\text{ta,eff}} r^3} \\ &= -\frac{3}{10} H_0^2 l^2 \left(\frac{\Omega_{\text{ta,eff}}}{b} + \Omega_\Lambda b^2 \right). \end{aligned} \quad (\text{A15})$$

The total energy per unit mass in the perturbation at maximum expansion is merely this potential energy, at $b = 1$. Of course, the kinetic energy is zero at maximum expansion.

Table A1. Spherical collapse model predictions

Model	Ω_0	Ω_Λ	redshift	$1 + \delta_{\text{vir}}$	δ_{f}
SCDM	1.0	0.0	0	177.7	1.686
			3	177.7	1.686
OCDM	0.5	0.0	0	278.1	1.667
			3	203.8	1.680
TACDM	0.4	0.6	0	286.2	1.678
			3	199.2	1.686

CHDM-2 ν and TCDM are identical to SCDM because the spherical collapse model depends only on Ω_0 , Ω_Λ and the redshift z , which are the same for these models.

After virialization, the potential energy is given by equation (A15) with b replaced by b_{vir} . The kinetic energy per unit mass is given by the virial theorem for a collection of particles,

$$2T = \sum_i v_i^2 = \sum_i \vec{r}_i \cdot \vec{\nabla}_{\vec{r}_i} U \quad (\text{A16})$$

(Landau & Lifshitz 1976, for example). The result is

$$T_{\text{vir}} = \frac{3}{10} H_0^2 l^2 \left(\frac{\Omega_{\text{ta,eff}}}{2b_{\text{vir}}} - 3\Omega_\Lambda b_{\text{vir}}^2 \right). \quad (\text{A17})$$

The total energy per unit mass after virialization is then

$$E_{\text{vir}} = T_{\text{vir}} + U_{\text{vir}} = -\frac{3}{10} H_0^2 l^2 \left(\frac{\Omega_{\text{ta,eff}}}{2b_{\text{vir}}} - 2\Omega_\Lambda b_{\text{vir}}^2 \right). \quad (\text{A18})$$

Equating to the energy per unit mass at maximum expansion and dividing out common terms gives

$$\frac{\Omega_{\text{ta,eff}}}{2b_{\text{vir}}} - 2\Omega_\Lambda b_{\text{vir}}^2 = \Omega_{\text{ta,eff}} - \Omega_\Lambda. \quad (\text{A19})$$

This is a reduced cubic equation for b_{vir} that can be solved by the cubic formula. Note that if $\Omega_\Lambda = 0$, the equation is linear and $b_{\text{vir}} = 1/2$, independent of Ω_0 . The density after virialization is merely equation (A11), with the scale factor adjusted for virialization, i.e.

$$\delta_{\text{vir}} = \frac{\rho_{\text{vir}}}{\bar{\rho}} - 1 = \frac{a^3}{b_{\text{vir}}^3} \frac{\Omega_{\text{ta,eff}}}{\Omega_0} - 1. \quad (\text{A20})$$

The values of δ_{vir} appropriate to models considered in this paper are shown in Table A1.

Note that our definition of δ_{vir} differs from that in Eke, Cole, & Frenk (1996) by $\Delta_{\text{ECF}} = \Omega(z) (\delta_{\text{vir}} + 1)$

A3 Evolution according to linear theory

For applications based upon linear theory, we would like to identify virialized regions according to the background universe, rather than the perturbation density. A canonical example is the Press-Schechter theory, where the cumulative probability of finding a ‘sufficiently high’ density peak is calculated using linear theory and a filter taken from the volume of background density needed to form an object of a given mass:

$$N(> M) = \sqrt{\frac{2}{\pi}} \frac{\delta_c}{\alpha_m} \int_r^\infty \frac{\epsilon(r')}{\sigma^3(r')} \exp \left[\frac{-\delta_c^2}{2\sigma^2(r')} \right] \frac{dr'}{r'^3}, \quad (\text{A21})$$

where

$$\epsilon(r) = \frac{1}{2\pi} \int_0^\infty k^3 P(k) W(kr) \frac{dW(kr)}{d(kr)} dk, \quad (\text{A22})$$

$$\sigma^2(r) = \frac{1}{2\pi^2} \int_0^\infty k^2 P(k) W^2(kr) dk, \quad (\text{A23})$$

$$W(x) = \begin{cases} \frac{3}{x^3} [\sin(x) - x \cos(x)] & \text{tophat} \\ e^{-x^2/2} & \text{Gaussian} \end{cases}, \quad (\text{A24})$$

$$r = \left(\frac{M}{\alpha_m \rho \Omega_0} \right)^{\frac{1}{3}}. \quad (\text{A25})$$

and α_m is $4\pi/3$ for a tophat window function, and $(2\pi)^{3/2}$ for a Gaussian window function.

In this theory, δ_c is taken from the spherical overdensity model, but the integrand is based upon linear theory, which implies that the bounds should be also.

Consider the evolution of a spherical overdensity at *early* times, when the dynamics are linear. Then, we can ignore the cosmological constant Ω_Λ (because it is third order in a and b), and expand the Friedmann equation (equation A4) and both expansion factors to first order in Ω_k and $\Omega_{k,\text{eff}}$. The Friedmann equation for the background universe reduces to

$$\dot{a} \approx H_0 \sqrt{\frac{\Omega_0}{a}} + \Omega_k \approx H_0 \sqrt{\frac{\Omega_0}{a}} \left(1 + \frac{\Omega_k}{2\Omega_0} \right). \quad (\text{A26})$$

Solving gives

$$\int_0^t dt' \approx \frac{1}{H_0 \Omega_0^{1/2}} \int_0^a da' a'^{1/2} \left(1 - \frac{\Omega_k}{2\Omega_0} a' \right) \quad (\text{A27})$$

$$a \approx \left(\frac{3H_0 t \Omega_0^{1/2}}{2} \right)^{2/3} \left[1 + \frac{\Omega_k}{5\Omega_0} \left(\frac{3H_0 t \Omega_0^{1/2}}{2} \right)^{2/3} \right]. \quad (\text{A28})$$

The early-time evolution for b is exactly the same, with Ω_0 replaced by $\Omega_{\text{ta,eff}}$ and Ω_k replaced by $\Omega_{k,\text{eff}}$. Plugging into equation (A20) and keeping terms up to next-to-lowest order gives

$$a^3 = \left(\frac{3}{2} H_0 t \right)^2 \Omega_0 \left[1 + \frac{3}{5} \frac{\Omega_k}{\Omega_0} \left(\frac{3}{2} H_0 t \right)^{2/3} \Omega_0^{1/3} \right], \quad (\text{A29})$$

$$b^{-3} = \frac{\left[1 - \frac{3}{5} \frac{\Omega_{k,\text{eff}}}{\Omega_{\text{ta,eff}}} \left(\frac{3}{2} H_0 t \right)^{2/3} \Omega_{\text{ta,eff}}^{1/3} \right]}{\left(\frac{3}{2} H_0 t \right)^2 \Omega_{\text{ta,eff}}}, \quad (\text{A30})$$

$$\frac{\rho}{\bar{\rho}} \equiv \delta_i + 1 \approx 1 + \frac{3}{5} \left(\frac{3}{2} H_0 t \right)^{2/3} \left[\frac{\Omega_k}{\Omega_0^{2/3}} - \frac{\Omega_{k,\text{eff}}}{\Omega_{\text{ta,eff}}^{2/3}} \right], \quad (\text{A31})$$

and

$$\delta_i = \frac{3}{5} a \left[\frac{\Omega_k}{\Omega_0} - \frac{\Omega_{k,\text{eff}}}{\Omega_{\text{ta,eff}}^{2/3} \Omega_0^{1/3}} \right]. \quad (\text{A32})$$

We can linearly evolve this overdensity to a later expansion factor a_f using the linear growth factor $D(a)$ normalized so $D \approx a$ for small a ,

$$\delta_f = \frac{3}{5} D(a_f) \left[\frac{\Omega_k}{\Omega_0} - \frac{\Omega_{k,\text{eff}}}{\Omega_{\text{ta,eff}}^{2/3} \Omega_0^{1/3}} \right], \quad (\text{A33})$$

where $D(a)$ is given by Padmanabhan (1993, equation 4.161), renormalized and converted so that the integrated variable is the expansion factor a ,

$$D(a) = \frac{5}{2} \Omega_0 \frac{\dot{a}}{a} \int_0^a \frac{da}{\dot{a}^3}, \quad (\text{A34})$$

and \dot{a} is given by the Friedmann equation (equation A4), as before. Values of δ_f appropriate to the models considered in this paper are shown in table A1. Note that we do not use these values elsewhere in the paper, but opt to use δ_f as a fitted parameter in the Press-Schechter approximation.

A Fortran-77 program that calculates $1 + \delta_{\text{vir}}$ and δ_f for any Friedmann cosmology and at any redshift may be downloaded from <http://fizzie.gsfc.nasa.gov/#cosmotools>. Several other programs of general interest, such as a general calculation of the linear fluctuation growth factor and the age of the universe are also available at the same site.